ISAS - INTERNATIONAL SCHOOL FOR ADVANCED STUDIES

The X-Ray Background synthesis model and the implications for the Unification Model

Fulvio Pompilio

International School for Advanced Studies (SISSA-ISAS)
Via Beirut 2-4, I-34013, Trieste, ITALY

Supervisors: Prof. L. Danese and Dr. G. Granato

Thesis submitted for the degree of "Magister Philosophiæ"

November 2001

***

To my beloved parents and

to Marzia and Sergio

***

Contents

List of Figures

List of Tables

Chapter 1

Introduction

1.1 The X-Ray Background

Since the discovery of the cosmic X-Ray Background (XRB) in the early sixties (Giacconi et al. 1962), a great deal of effort has been made to understand its origin (for a review see Fabian & Barcons 1992).
The wide XRB emission extends over more then five decades of energy ranges, namely from X-rays up to γ-rays, the bulk of its intensity peaking at around 30 keV. However, the XRB characteristics depend on the energy band.
Indeed, in the soft X-rays (below 2 keV), the emission is anisotropic (Tanaka & Bleeker 1977). Specifically, the 0.1-0.5 keV emission is probably due to the galactic local bubble with a temperature of about 10^6 K; in the 0.5-0.9 keV the main contributor is hot gas ($T \sim 2.2 \times 10^6$ K) in our Galaxy (Hasinger 1992; Wang & McCray 1993).
On the other hand, above 2 keV the XRB has a highly uniform extra-galactic emission and an excess component along the Galactic plane (Koyama 1989). As concerns the origin of this purely extra-galactic emission, the spectrum resembles that of a hot plasma at about 40 keV (Marshall et al. 1980; Rotschild et al. 1983) and can be analytically described as (Boldt 1987):

$$I(E) = \begin{cases} 7.877\ E^{-0.29} e^{-E/41.13} & \text{if } 3 < E < 60\ keV \\ 1652\ E^{-2.00} + 1.754\ E^{-7.00} & \text{if } 60\ keV < E < 6\ MeV \end{cases} \qquad (1.1)$$

as reported in Figure 1.1; a compilation of the best available data about the XRB can be seen in Figure 2.6 in Chapter 2.
Though it seemed to be a straightforward interpretation, the hypothesis of

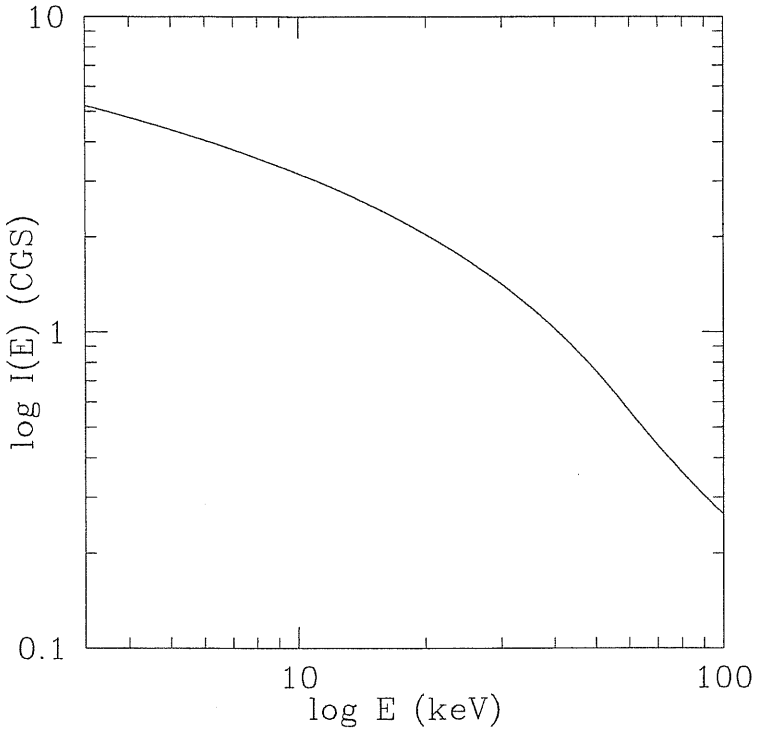

Figure 1.1: The intensity spectrum of the hard XRB as parametrized in Boldt (1987) (I(E) is in units of $keV\ cm^{-2}s^{-1}sr^{-1}keV^{-1}$).

a hot plasma had to be discarded since a hot intergalactic medium would produce distortions in the cosmic microwave background (CMB) through inverse Compton scattering, which is excluded by COBE data (Mather et al. 1994). Indeed, the comptonization parameter for an intergalactic medium (IGM) with a fractional emission intensity f, a temperature T_8 (in units of 10^8 K) and emitting at a median redshift z_e can be expressed as (Peebles 1993):

$$y \simeq 2 \times 10^{-4} \frac{(1+z_e)^2 f^{1/2} {T_8}^{5/4}}{C^{1/2} h_{50}^{1/2} \Omega^{1/4}} \tag{1.2}$$

where Ω is the baryonic fraction, h_{50} is the Hubble constant in units of 50 $km\ s^{-1} Mpc^{-1}$ and C is the *clumping factor* defined in terms of the electron density n_e (the symbol $\langle\rangle$ denotes the average):

$$C \equiv \frac{\langle n_e^2 \rangle}{\langle n_e \rangle^2}. \tag{1.3}$$

If a median redshift for the XRB production of $z_e < 5$ is assumed and a value of C consistent with the diffuse medium hypothesis is considered, then the value of y is highly exceeding the measured value of $y \leq 2.5 \times 10^{-5}$ (Mather et al. 1994).
The alternative is that the XRB is produced by discrete sources emission. The candidate sources must be searched for among the following:

- **galaxies**: in a normal galaxy, the X-ray emission is mainly provided by X-ray binaries, Supernovae remnants and hot gas, the latter basically emitting in the soft band, yet. Therefore, the X-ray activity is deeply connected to stellar processes and evolution, so that physical parameters, such as the age of the galaxy, are fundamental tracers of their contribution to the XRB. It must be noted that X-ray activity in galaxies, which has usually been considered quite low, on the converse could be important, as *Chandra* data are showing (to be discussed throughout this work);

- **clusters**: their X-ray emission is due to thermal breemstrahlung from hot gas trapped in the gravitational potential well; however, the bulk of the emission is provided in the soft band and the hard XRB contribution is of order of a few per cent, e.g. $\sim$ 3 % in the 4-12 keV band (Fabian & Barcons 1992);

- **Active Galactic Nuclei (AGN)**: they are the best candidate, being the most luminous X-ray sources and having a suitable X-ray spectrum and redshift evolution, which combine to reproduce the XRB; for this reason, the XRB synthesis models have usually invoked AGN as the most promising tool and this is the approach of this work, as well.

As regards AGN, yet it must be noted that the nature of the sources producing the hard XRB undergoes the so-called "spectral paradox", i.e. a discrepancy between the XRB spectral slope ($\alpha = 0.4 - 0.5$, Gendreau et al. 1995; Chen, Fabian & Gendreau 1997; Vecchi et al. 1999) and that of bright AGN in the same band ($\alpha = 0.7 - 0.9$, Turner & Pounds 1989; Nandra & Pounds 1994; Nandra et al. 1997). The puzzle is solved if a mixture of absorbed (type 2 AGN) and unabsorbed (type 1 AGN) is considered, the absorbing column density determining the observed spectral slope (Setti & Woltjer 1989), as will be extensively described further.
However, additional complications to the above scenario have come from recent data.
The recent optical identification breakthrough of *Chandra* sources have demonstrated that part of the newly discovered XRB sources may be quite different from established classes of AGN. Whether they are optically luminous X-ray active normal galaxies or AGN precursors in a pre-quasar/Seyfert state of obscured growth of the massive black hole (Fabian 1999), nevertheless they are found to hardly populate soft X-ray surveys or shallow hard X-ray surveys and deep pointings in the hard band are required to observe them, as discussed in this work.
Therefore, our picture of the X-ray sky should be lacking of relevant peculiarities, which could be investigated through hard X-ray surveys. This is the motivation and the approach followed hereafter in this work.

1.2 AGNs and the Unification Model

Many synthesis models for the XRB have been developed over the last decade, based on integrated emission from AGN (Setti & Woltjer 1989; Madau et al. 1994; Matt & Fabian 1994; Celotti et al. 1995; Comastri et al. 1995; Gilli, Risaliti & Salvati 1999; Pompilio, La Franca & Matt 2000), where the combination of type 1 and type 2 AGN (respectively AGN1 and AGN2) is the cornerstone in reproducing the spectral shape of the XRB. Therefore, it is important to give a few details about AGN1/AGN2 distinction.

Radio power	Optical lines properties	Inclination angle
RQ	Sy2 + Sy1	high / low
RL	NLRG + BLRG	high / low

Table 1.1: The basic AGN taxonomy as interpreted by the UM in terms of an edge-on (i.e. high inclination angle) or face-on view of the galaxy.

From a physical point of view, the difference among AGN1 and AGN2 is ascribed to the amount of absorbing matter and is modeled in terms of the relative orientation of the line of sight with respect to the obscuring matter surrounding the central engine, generally considered to be arranged in a toroidal geometry (Antonucci & Miller 1985). This is depicted in Figure 1.2, where at the very center there is the supermassive black hole, surrounded by the small accretion disc and the big dusty torus; the black spots are the Broad Line Region (BLR) clouds, while the grey ones are the Narrow Line Region (NLR) clouds and the black dots are diffuse ionized plasma; for completeness, the jets are sketched, as well. This physical structure, as combined with the relative orientation of the line of sight, is the basis of the widely accepted paradigm known as the Unification Model (UM).
From an observational point of view, AGN1 and AGN2 are distinguished by their optical emission lines, the former showing both broad and narrow lines, the latter lacking broad lines. The UM can interpret the difference and can be stated as follows:

the observation of broad lines is related to the relative position of the observer, which could result in the BLR emission being absorbed by the torus; on the converse, the NLR is located on much larger scale and is not affected by torus reprocessing.

The combination of physical structures and orientation provides the wide taxonomy of AGN, as described in Table 1.1. AGN can be divided according to their radio power and the *radio-loud* ($L_R/L_O > 10$) can appear as Narrow Lines Radio Galaxies (NLRG) or Broad Lines Radio Galaxies (BLRG), owing to their lines properties. On the other hand, the *radio-quiet* are respectively type 2 Seyfert Galaxies (Sy2) and and type 1 Seyfert Galaxies (Sy1). No lines are observed in the most extreme objects, namely Optically Violent Variables (OVV, typically *radio-quiet*) and blazars (*radio-loud*).

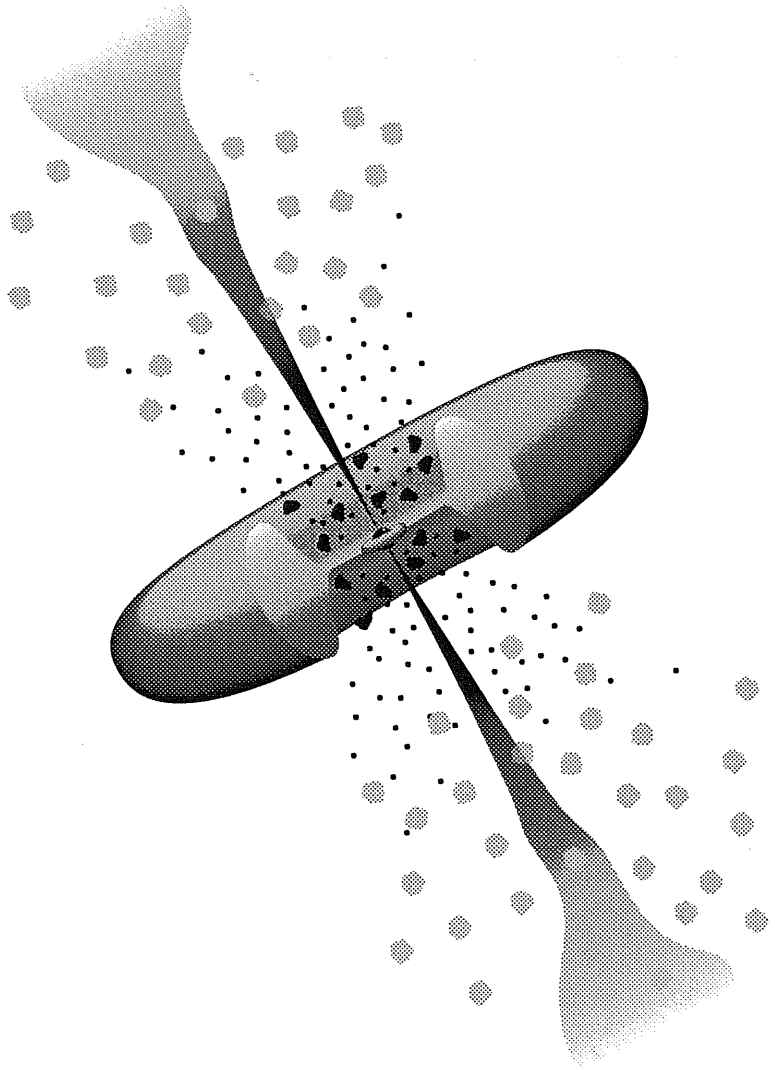

Figure 1.2: The qualitative geometry of an AGN (see text for a description).

1.3 The UM in the X-rays

A strict correspondence can be made between physical structures and different observations of AGN, according to the UM.
Historically, the observational segregation among type 1 and type 2 AGN has been marked by the presence and characteristics of polarized optical emission lines (broad / narrow). Nevertheless, such a separation is also found in other wavelengths, namely in Radio, IR and X-rays bands.
Since this work is focused on the XRB, further details about the X-ray interpretation of the UM are given below. They are one of the basic assumption of the model described in Chapter 2.
The X-rays in AGN are produced by accretion onto the disc and make their way out of the inner core of the galaxy along a path eventually piercing through the molecular torus (Figure 1.2), owing to the observer's line of sight.
The wideband X-ray emission can be divided into a soft band ($E < 1$ keV) and a hard band ($E > 1$ keV). If the line of sight passes through the torus, photoelectric absorption and Compton scattering will affect the incident radiation, absorbing the low-energy radiation up to a threshold energy which is fixed by the torus column density (see Figure 2.1 in Chapter 2 and related text).
The UM states that an AGN1 is seen close to the BLR axis, i.e. face-on, while an AGN2 is seen close to the plane of the galaxy, i.e. edge-on, so that the spectral features of the two sources can be roughly interpreted as follows:

- AGN1: the X-ray spectrum exhibits both the soft and the hard bands;
- AGN2: the soft band and eventually the low-energy tail of the hard band spectra are absorbed, depending on the value of the torus column density; part of the soft spectrum can be scattered along the line of sight by the diffuse ionized plasma surrounding the central engine (black dots in Figure 1.2).

These are the main signatures of the X-ray spectrum, marking the type 1 / type 2 segregation. As regards the X-ray regime, there are two other features worth stressing:

- soft-excess: a soft energy excess with respect to the primary spectrum may be present, whose origin is still debated, probably to be ascribed to the high-energy tail of the disc thermal emission;

- Fe K_α line: it is thought to arise from the disc and/or the inner wall of the torus when hit by the primary radiation.

Actually, the radiation reflected by the disc / torus and providing the Fe K_α line also adds a reflection component to the overall spectrum, which typically flattens the slope at intermediate energies.
Last, the radiation piercing through the torus will undergo Compton down-scattering and part of it will eventually emerge as a transmitted component. It is an important characteristics of AGN2 spectrum and will be discussed further in Chapter 2, where a sketch of AGN1 / AGN2 X-ray spectra can be found, as well, in Figure 2.3.

1.4 Hard X-ray surveys

The reason to perform hard X-ray surveys is to sample the energy range where the XRB starts to present its purely extra-galactic nature and the bulk of its intensity is produced.
A few satellites were devoted to this aim in the last decade:

- **HEAO1-A2** (Piccinotti et al. 1982): flux limit of $3\times10^{-11} erg\ cm^{-2}s^{-1}$;
- ***Ginga*** (Kondo 1990): flux limit of $8 \times 10^{-12} erg\ cm^{-2}s^{-1}$;
- **ASCA Surveys**: up to a flux limit of $4 \times 10^{-14} erg\ cm^{-2}s^{-1}$;
- **BeppoSAX Surveys**: up to a flux limit of $5 \times 10^{-14} erg\ cm^{-2}s^{-1}$;
- **ASCA-ROSAT Surveys**;
- **BeppoSAX-ROSAT Surveys**;

where the flux limits refer to the 2-10 keV band.
The ASCA satellite achieved the sensitivity to detect faint sources with a flux limit of a few $10^{-14} erg\ cm^{-2}s^{-1}$ in the 2-10 keV band, resolving nearly 30 % of the XRB in that band.
In particular, the ASCA Large Sky Survey (LSS) (Ueda et al. 1998; Ueda et al. 1999a) down to a flux limit of $10^{-13} erg\ cm^{-2}s^{-1}$ (2-10 keV), resolved 23 ± 3 % of the XRB mainly into AGN, with an average spectral index of $\alpha = 0.49 \pm 0.10$, consistent with the XRB one and suggesting that hard sources become significant at that flux level.

The above results were confirmed by the ASCA Medium Sensitivity Survey (AMS or GIS project, Takahashi et al. 1998; Ueda et al 1999b), with a flux limit of $7 \times 10^{-14} erg\ cm^{-2} s^{-1}$. Specifically, the spectral hardening at fainter fluxes has been confirmed by different analysis by many authors (Della Ceca et al. 1999; Ogasaka et al. 1998), which is one of the most important result achieved by ASCA within this context.
In agreement with this, the survey performed by BeppoSAX in the 2-10 keV band (Giommi, Perri & Fiore 2000) resolved about 25 % of the XRB at a flux limit of $5 \times 10^{-14} erg\ cm^{-2} s^{-1}$, extended to $1.5 \times 10^{-14} erg\ cm^{-2} s^{-1}$ through a complementary fluctuations analysis (Perri & Giommi 2000) and resolving 40-50 % of the XRB. The hardening at faint fluxes has been confirmed and is ascribed to an increasing percentage of absorbed sources at faint fluxes, rather than to a gradual spectral flattening.
Another support comes from preliminary XMM-*Newton* observation of the Lockman Hole (Hasinger et al. 2001), reaching a flux limit of $1.4 \times 10^{-15} erg\ cm^{-2}\ s^{-1}$ (2-10 keV) and showing a 40 % fraction of the sources marked by hard X-ray spectra.
Anyhow, the most crucial results are coming from the *Chandra* satellite. Due to the low flux limit ($3.2 \times 10^{-15} erg\ cm^{-2} s^{-1}$, 2-10 keV), Mushotzky et al. (2000) found in the SSA 13 field an unexpected population identified with apparently normal galaxies, contributing roughly one third to the total number counts. Moreover, *Chandra* observation of the Deep Field South (CDFS) ($2 \times 10^{-15} erg\ cm^{-2} s^{-1}$, 2-10 keV) found a similar significant fraction of normal galaxies (Giacconi et al. 2001).
The implication of these findings (particularly regarding the CDFS) will be discussed in what follows.

1.5 The present work overview

In a previous work (Pompilio, La Franca & Matt 2000, hereafter PLM00), a synthesis model for the XRB was presented, relying on two key assumption: first, the high energy XRB is mainly produced by AGN; second, AGN1 and AGN2 fulfill the UM scenario.
As a result, it was found that a significant deviation from the observed local Universe AGN2 percentage is needed not to over produce the XRB, namely the AGN2 to AGN1 ratio is deeply decreased above $z > 1$ with respect to the observed local value AGN2/AGN1$\simeq$ 4.

The aim of this work is to obtain further inspections in the above results, with particular interest to those clues which can be gained through recent observations, e.g. new hard X-ray surveys.
To introduce the model, the main features and results of PLM00 are reviewed in Chapter 2.
The leading part concerns the number counts evaluation as a function of redshift in the 2-10 keV band and the discussion of the differences among PLM00 (*R(z) model*) and the "standard" scenario, i.e. a fixed ratio independent on redshift. This is presented in Chapter 3.
Since the possibility of facing the new X-ray surveys results is a fundamental goal, the expectation of the model from hard X-ray surveys is considered and the general X-ray sky overview emerging from it is sketched in Chapter 3, as well.
Last, consequences, interpretations and possible perspectives are discussed in Chapter 4.

Chapter 2

The XRB synthesis model

2.1 AGN spectra

The X-ray emission of AGN has been modeled as a weighted combination of AGN1 and AGN2 spectra, according to the PLM00 model (to refer to for more details).
The template spectrum for the AGN1 is the sum of a power law primary spectrum ($\alpha_2 = 0.9$) with an exponential cut-off ($E_c = 400$ keV), plus a Compton reflection component $F_r(E)$, which is likely to emerge from the accretion disc and assumes an average inclination of 60°. As discussed in PLM00, the inclusion of a soft excess, i.e. a steeper ($\alpha_1 = 1.3$) low-energy (E<1.5 keV) component, has been considered and discussed. However, since this work is focused on hard X-rays, the soft excess will be assumed without any further investigation.
The general AGN1 spectral shape is then fixed as the following:

$$F_{AGN1} = \begin{cases} E^{-\alpha_1} & \text{if } E < 1.5\ keV \\ E^{-\alpha_2} e^{-E/E_c} + F_r(E) & \text{if } E > 1.5\ keV \end{cases} \tag{2.1}$$

For the sake of simplicity, the Fe K_α emission line has not been included in the above formulation, though it is a common feature in AGN1, as mentioned in the previous Chapter. This choice is justified by the fact that the line emission is smeared-out by redshift integration, so that the XRB results to be smooth (Schwartz 1992). Moreover, the iron line contribution to the XRB is below 5 % in the 1.5-7 keV band and its peak intensity is below 7 % at 2 keV (Gilli et al. 1999).

According to the UM, AGN2 have the same AGN1 primary spectrum, obscured by an amount of intervening gas. Its neutral hydrogen column density distribution can be written as a fair analytical approximation of the observed one (Risaliti, Maiolino & Salvati 1999) and was fixed as:

$$\frac{dN\ (logN_H)}{d\ \log\ N_H} \propto log\ N_H \tag{2.2}$$

where the range is $10^{21} \leq N_H \leq 10^{25}\ cm^{-2}$.
A key role in AGN2 was played by the transmitted component of the input spectrum through the absorbing matter, provided by Compton down-scattering of high energy photons. This physical mechanism is relevant as $N_H > 10^{23}\ cm^{-2}$ and the competition among absorption and down-scattering determines the emergent spectrum. The threshold energy separating the dominance of the two phenomena can be seen in Figure 2.1.
It should be noted that for high column densities ($N_H \geq 10^{24}\ cm^{-2}$), the X-ray emission emerges above 10 keV, the bulk of it being at $\sim$ 30 keV, as shown by Monte Carlo simulations (Matt, Pompilio & La Franca 1999). In order to better clarify this point, in Figure 2.2 the spectrum transmitted through a $N_H = 3 \times 10^{23}\ cm^{-2}$ absorber is reported. Actually, the bulk of the emission corresponds to the peak of the XRB intensity, therefore low to moderate redshift absorbed sources are likely to be crucial for the XRB production.
Then, the absorbed component has been averaged over the N_H distribution and the resulting AGN1 and AGN2 spectra are sketched in Figure 2.3.
Last, the total template spectrum (AGN1+AGN2) has been weighted by the relative ratio $R \equiv AGN2/AGN1$, according to:

$$F(E) = F_{AGN1} + R \times F_{AGN2} \tag{2.3}$$

where the estimated local value is $R = 4.0 \pm 0.9$ if Seyfert 1.8 - 1.9 and Seyfert 1.2 - 1.5 are respectively classified as AGN2 and AGN1 (e.g. Maiolino & Rieke 1995).

2.2 AGN evolution

The other important parameter concerns the Luminosity Function in the X-rays (XLF), which was chosen as the one derived by Boyle et al. (1994) from

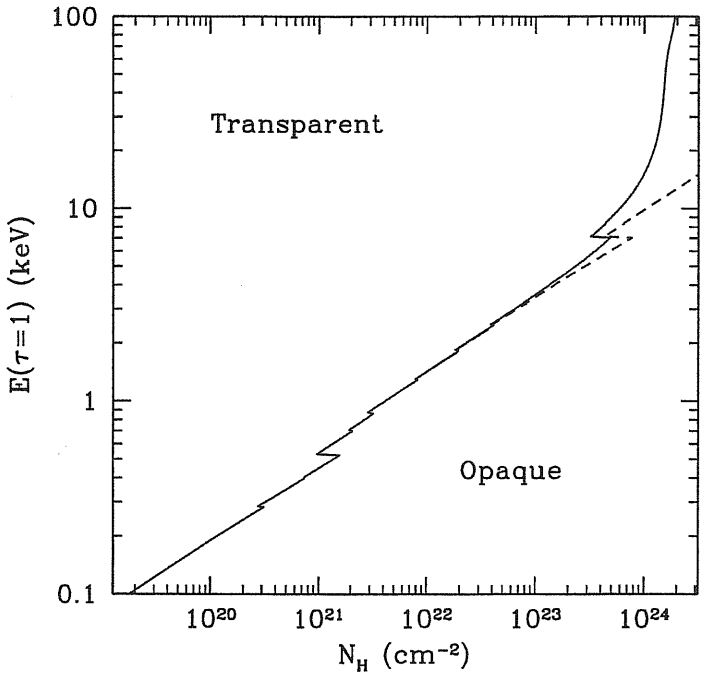

Figure 2.1: The threshold energy of the transmitted component as a function of the column density. The solid line fixes $\tau = 1$; the dashed line refers to the photoelectric absorption (Matt 1998).

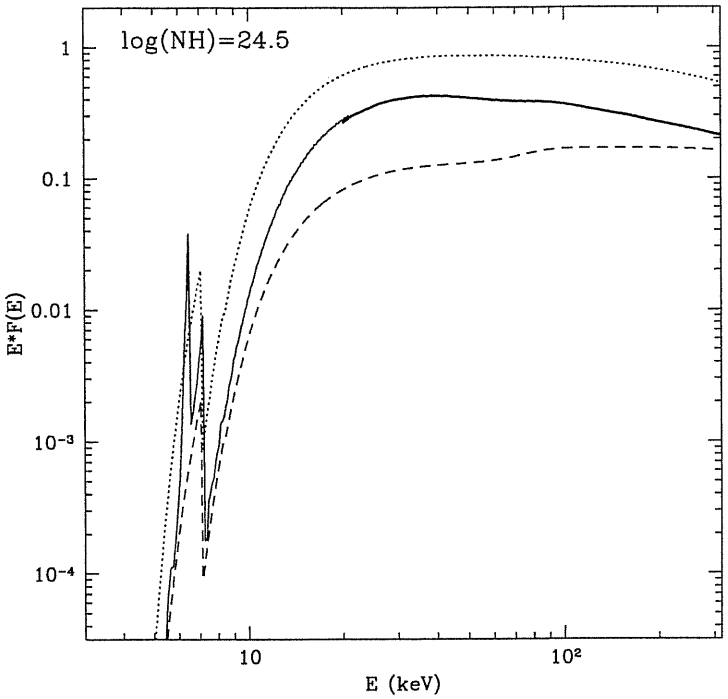

Figure 2.2: The spectrum of a power law incident spectrum passing through an absorber with $N_H = 3 \times 10^{24}\ cm^{-2}$ if Compton down-scattering is considered (solid line), or if only photoelectric absorption (dotted line) or photoelectric + Compton absorption without down-scattering (dashed line) are allowed.

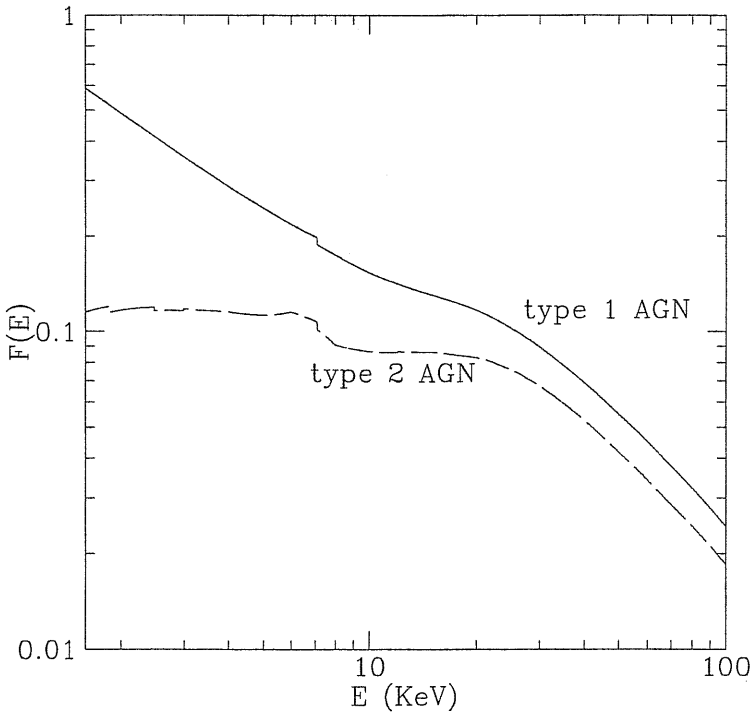

Figure 2.3: The assumed spectrum for AGN1 and AGN2, as described in the text. The sharp edge at 7.1 keV is due to Fe K absorption edge.

ROSAT (0.5-2.0 keV) and *Einstein* (0.3-3.5 keV) AGN1 surveys.
Indeed, the best suited hard XLF is still lacking, few attempts to evaluate it being severely affected by poor statistics, so far (Boyle et al. 1998). New results about it are likely to come in the near future from the HELLAS survey data supply based on BeppoSAX data (La Franca et al. 2001, see also Chapter 4). So far, as the most reasonable approach, the soft XLF was considered and extended to the hard X-ray range.
It must be noted that the soft XLF is retained to be well known at low and intermediate redshift, while at high redshift ($z \geq 3$) insufficient sampling and lack of statistics prevent the XLF from being firmly evaluated. Anyhow, AGN1 in the X-rays are detected up to $z > 4$ (e.g. $z = 4.6$, Miyaji, Hasinger & Schmidt 1998) and no evidence for a space density turn-over is found up to $z \sim 3$.
A further complication concerns the AGN2 XLF, which is not available due to the paucity of secure AGN2 identifications. Then, the same AGN1 XLF has been applied to AGN2, renormalizing by the relative percentage R. This is the most direct assumption if the UM holds at every redshift.
The basic motivation for the choice of the Boyle et al. (1994) XLF was that it is the less affected AGN1 XLF by the possible presence of AGN2 being detected in the soft band. Therefore, it provides a good tool to apply the UM. Indeed, as specified above, it was considered for AGN1 and then extended to AGN2 weighting for a relative percentage factor and implicitly assuming the N_H distribution to be independent of the source luminosity.
The shape of it is a double power-law:

$$\begin{cases} \Phi = \Phi^* \; L_{44}^{-\gamma_1} & \text{if } L < L_{44}^* \\ \Phi = \Phi^* \; (L_{44}^*)^{(\gamma_1 - \gamma_2)} \; L_{44}^{-\gamma_2} & \text{if } L > L_{44}^* \end{cases} \tag{2.4}$$

where $\gamma_1 = 1.36$, $\gamma_2 = 3.37$, $L_{44}^* = 0.39$ (units of $10^{44} erg\ s^{-1}$), $\Phi^* = 1.45 \times 10^{-6} Mpc^{-3} (10^{44} erg\ s^{-1})^{-1}$ and describes a Pure Luminosity Evolution (PLE) scenario, with the break luminosity following:

$$\begin{cases} L_{44}^*(z) = L_{44}^*(z=0) \times (1+z)^k & \text{if } z < z_{max} \\ L_{44}^*(z) = L_{44}^*(z=0) \times (1+z_{max})^k & \text{if } z \geq z_{max} \end{cases} \tag{2.5}$$

where $k = 2.90$ and $z_{max} = 1.73$. A picture of its shape as a function of luminosity and redshift can be seen in Figure 2.4.
The XLF model fit parameters refer to a $H_0 = 50\ Km\ s^{-1} Mpc^{-1}$ and $q_0 = 0.5$ Universe and this cosmology is fixed throughout the paper. However,

no significant differences arise when choosing different cosmologies in what follows, namely the general results discussed here still hold.
In recent works, the soft XLF describing a PLE scenario has been questioned, due to the fact that a Luminosity Dependent Density Evolution (LDDE) seems to be the only acceptable fit to ROSAT surveys at different depths (Miyaji, Hasinger & Schmidt 2000). The effect of a LDDE is to flatten the faint end slope as redshift increases. Its functional shape can be described as follows:

$$\frac{d\Phi(L_X,z)}{d\ log\ L_X} = \frac{d\Phi(L_X,z=0)}{d\ log\ L_X} \times e(L_X,z)) \tag{2.6}$$

where:

$$\frac{d\Phi(L_X,z=0)}{d\ log\ L_X} = A[(L_X/L_*)^{\gamma_1} + (L_X/L_*)^{\gamma_2}]^{-1} \tag{2.7}$$

and the factor $e(L_X,z))$ is given by:

$$\begin{cases} (1+z)^{p_3} & \text{if } z \leq z_c; L_X < L_a \\ (1+z)^{p_1} & \text{if } z \leq z_c; L_X \geq L_a \\ e(L_X,z_c))\left[\frac{(1+z)}{(1+z_c)}\right]^{p_2} & \text{if } z > z_c \end{cases} \tag{2.8}$$

in which $p_3 \equiv max(0, p_1 - \alpha\ log\ [L_a/L_X])$.
However, the difference with respect to the PLE models regards the faint end, where sparse sampling cannot provide strong evidence of such a conclusion. Moreover, the sample analysis by Miyaji, Hasinger & Schmidt (2000) is affected by the presence of AGN2, though very few of them are present in ROSAT surveys. This makes the LDDE conclusion less appealing with respect to the Boyle et al. (1994), which is a secure determination of AGN1 XLF. Therefore, Miyaji, Hasinger & Schmidt (2000) XLF is not considered any further in this work, although other comments on LDDE models are discussed in the last Chapter.

2.3 The synthesis model and the results

The intensity of the XRB has been calculated according to:

$$I(E) = \int\int \frac{d^2N}{dVdL} \frac{F[E(1+z)]}{4\pi d_l^2} dLdV \tag{2.9}$$

having introduced the AGNs evolution ($\frac{d^2N}{dVdL}$) and spectrum corrected for the redshift and weighted in terms of AGN1 and AGN2 ($F[E(1+z)]$), where

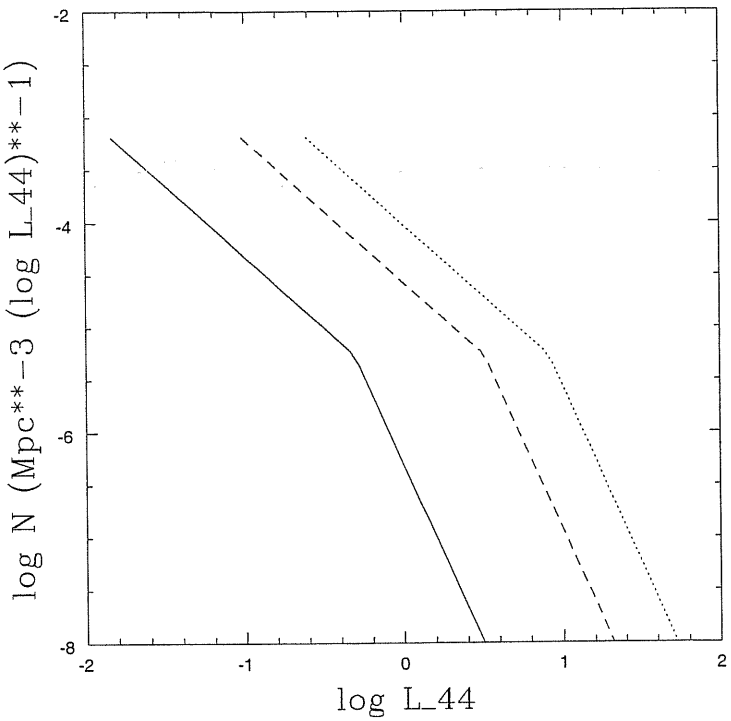

Figure 2.4: The XLF of Boyle et al. (1994) at different redshifts: $z = 0.1$ (solid line); $z = 1.0$ (dashed line); $z = 3.0$ (dotted line).

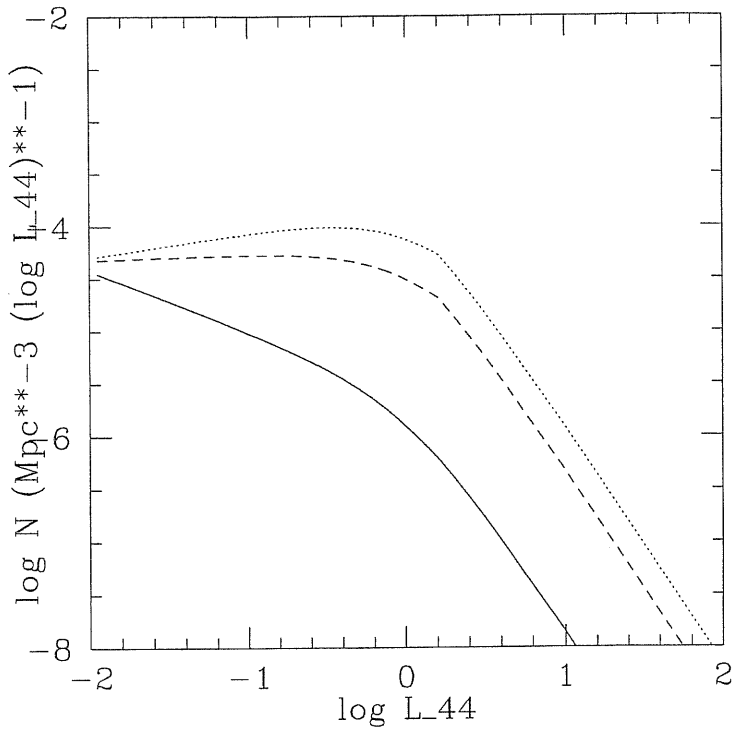

Figure 2.5: The XLF of Miyaji, Hasinger & Schmidt (2000) at different redshifts: $z = 0.1$ (solid line); $z = 1.0$ (dashed line); $z = 3.0$ (dotted line).

d_l is the luminosity distance and dV is the shell of the Universe of thickness dz, which depends on redshift according to the cosmological model. For $H_0 = 50\ Km\ s^{-1}Mpc^{-1}$ and $q_0 = 0.5$ it holds:

$$dV(z) = \left(\frac{c}{H_0}\right) \frac{4\pi d_l^2}{(1+z)^3(1+2q_0z)^{1/2}} dz. \tag{2.10}$$

The best fit result is sketched in Figure 2.6 and is obtained allowing for a redshift dependent variation of the AGN1/AGN2 ratio. Indeed, the main result in PLM00 was that, in order not to over produce the XRB, the relative percentage of AGN2 must be a sensitive function of redshift.
The functional shape for $R \equiv \frac{N(AGN2)}{N(AGN1)}$ was fitted as:

$$R(z) = R(z=0) \times (1+Z)^{\alpha_1} e^{\alpha_2\ Z} \tag{2.11}$$

where $\alpha_1 = 1.28 \pm 0.04$ and $\alpha_2 = -0.89 \pm 0.03$ (the quoted errors refer to 68% confidence level), that is sketched in Figure 2.7.
Specifically, it is quite constant below $z = 1$ and then decreases steeply. Note that, as discussed in PLM00, the constant trend is pushed slightly towards higher redshift and the decrease is more dramatic if a $\sim 30\%$ higher normalization to the hard XRB is considered, as outlined by some authors (Vecchi et al. 1999). However, as a conservative approach, the above shape is fixed in the following.
The main reason for the fitting result can be ascribed to the assumed AGN2 spectrum. In fact, the inclusion of the transmitted component significantly hardens the spectrum and extends it to higher energies. Combining this peculiarity with the energy band shift due to redshift, the AGN2 contribution can over produce the XRB if their number is not reduced as redshift increases, resulting in the $R(z)$ effect. On the other hand, the functional shape of $R(z)$ is XLF dependent, in the sense that any modification to the AGN1 XLF assumed by the model corresponds to an AGN2 number variation, affecting the $R(z)$ factor. Therefore, it is reasonable to ask how much is the model result really bound to the choice of that particular XLF, or else how long this result can hold if the XLF is modified by more recent estimate.
To have further inspection in this point, the preliminary results on HELLAS BeppoSAX survey data for the 2-10 keV AGN1 XLF (La Franca et al. 2001) can provide the most recent evaluation of the hard XLF (see Chapter 4). That analysis shows consistency with the PLE previous estimates (Boyle et

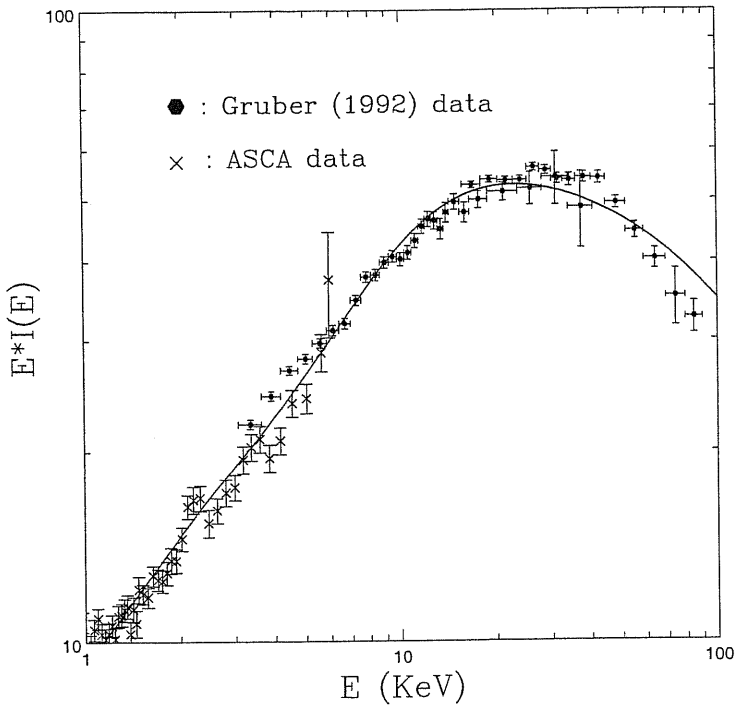

Figure 2.6: The best fit of the $R(z)$ model to the available data on the XRB.

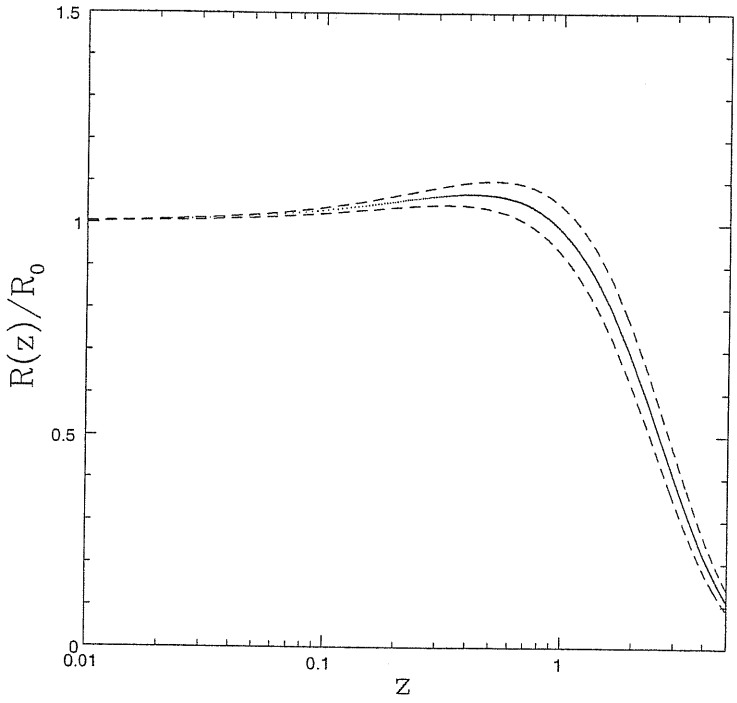

Figure 2.7: The $R(z)$ parameter normalized to the local value (solid line); the dashed lines represent the 68% confidence level.

al. 1998), though a slightly higher evolution, i.e. higher value of the parameter k in eq. (2.4). However, the main difference is a higher normalization, as follows from the necessity of better fitting the observed higher density of faint AGN1 at high redshifts. Then, it is likely that such an increase can eventually constrain the $R(z)$ model to a steeper decrease, to face with the excess of AGN2 emission in reproducing the XRB. Further discussion about the XLF can be found in Chapter 4.
As a conclusion, the up-coming results on the XLF should strengthen the $R(z)$ model, although the functional shape depends on the spectra and evolution assumed, so that it can change with the XLF.
The consequences of the introduction of the $R(z)$ model on number counts and possible interpretations to it are the subject of the rest of this work.

Chapter 3

The number counts

3.1 Theoretical prediction

The number counts as theoretically predicted by the $R(z)$ model have been evaluated in the 2-10 keV band as a function of the sampling flux limit and compared to the expected values from the $R = const$ model.
It must be noted that a flux-limited sample will tend to bias AGN2 detection, owing to their fainter emission with respect to AGN1. This effect is also recovered in the $R = const$ model, which is found to deviate from the assumed local AGN2 percentage of 0.8, decreasing to nearly 0.6 at $F_{lim} = 10^{-15} erg\ cm^{-2} s^{-1}$. Therefore, it is important to remind this while searching for any $R(z)$ signature in data inspection.
However, the AGN2 percentage values are quite lower than expected from the $R = const$ model, its value being 0.47 at $F_{lim} = 10^{-15} erg\ cm^{-2} s^{-1}$, so that such an effect is likely to be observable, once a significant statistics is provided.
Two trends are worth being remarked:

- the departure among the two is increased by lowering the flux-limit;
- as the flux limit becomes brighter, the peak in the number counts shifts to lower redshift values.

These trends are expected due to the combination of redshift and flux limit as an indicator of the sampling depth. Namely, the lower the flux limit, the higher the redshift so that the $R(z)$ effect is more clearly seen. On the converse, the higher the flux limit, the lower the redshift and the number counts

Flux limit (CGS)	AGN2 percentage
10^{-15}	0.47
5×10^{-16}	0.48
10^{-16}	0.48
5×10^{-17}	0.49
10^{-17}	0.49
5×10^{-18}	0.59
10^{-18}	0.68

Table 3.1: The relative AGN2 percentage as a function of the flux-limit (in units of $erg\ cm^{-2}s^{-1}$).

contribution will be dominated by local sources, i.e. the peak shifts to lower redshift values.
Yet, this trend stops at a certain threshold flux and actually it reverses at $F_{lim} \sim 10^{-17} erg\ cm^{-2}s^{-1}$, namely the AGN2 percentage turns to increase, as can be seen in Table 3.1.
It can be ascribed to a *saturation effect* of the model: the high redshift sampling is overwhelmed by the replenishment from faint local AGN2, which are over abundant, so that the ratio becomes mainly sensitive to the $z < 1$ sources.
Indeed, this effect is enhanced if the faint end slope of the XLF, where most of AGN2 resides, is varied, in the sense that steeper slopes (i.e. more sources at a fixed luminosity) lead to the *saturation effect* at brighter fluxes.
This poses a severe limitation to the chance of discriminating among the $R(z)$ and the $R = const$ models through deep X-ray surveys, i.e. going to lower flux-limit. On the converse, any constraining check of the $R(z)$ model should come from statistically significant AGN sample, coming from wide surveys spectroscopical identifications, not yet at disposal for such an analysis.
A comparison with the number counts from the most recent X-ray surveys data is described throughout this Chapter.

3.2 The instrumental response

Since the most recent and complete data supply in the hard X-rays are coming from the *Chandra* satellite, in order to compare theoretical expectations to them, any complication arising from instrumental effects must be included. Indeed, turning to observational quantities, the instrumental response must be taken into account.
As concerns our task of facing with AGN1/AGN2 statistics, the most relevant issue is quantifying any bias in detecting a particular kind of source.
The instrumental response for the *Chandra* satellite strictly depends on the energy band. Specifically, the hard band exhibits a worse response with respect to the soft band ($E < 2$ keV) and this introduces a bias towards AGN2 detection, which can definitely be relevant in AGN1/AGN2 evaluation.
This is particularly clear from Figure 3.1, which sketches the AXAF CCD Imaging Spectrometer (ACIS) effective area $A(E)$ corrected by the quantum efficiency $QE(E)$ and the response matrix $R(E, PH)$. These quantities affect the count rate N detected by the instrument as follows (Allen et al. 1998):

$$N = \int_{PH_1}^{PH_2} dPH \int_{E_1}^{E_2} I(E)A(E)Q(E)R(E, PH)dE \tag{3.1}$$

where PH is the pulse height and $I(E)$ is the incident flux over the energy band fixed by E_1 and E_2.
As pursued by other authors (Gilli, Salvati & Hasinger 2001), a response convolution procedure of the model and the instrumental effective area was performed. The basic procedure evaluates an effective count rate to flux conversion factor by convolving the instrumental response with the assumed source spectrum in the integration of the source spectrum over the redshift-corrected energy band:

$$CR = \int_{\Delta E(z)} \frac{F(E)}{E} A_{corr}(E)dE \tag{3.2}$$

where $F(E)$ is the source spectrum and $A_{corr}(E)$ is the effective area corrected by the quantum efficiency and the response matrix.
The same factor has been found for the source spectrum used by Boyle et al. (1994) in evaluating the luminosity function (a simple power-law with energy index 1.0, denoted by $F_{XLF}(E)$):

$$CR_* = \int_{\Delta E(z)} \frac{F_{XLF}(E)}{E} A_{corr}(E)dE. \tag{3.3}$$

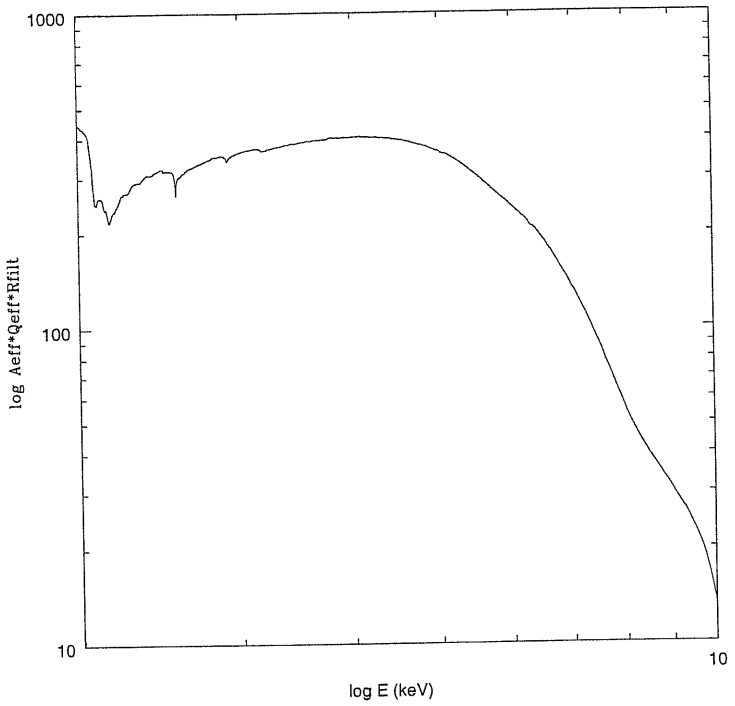

Figure 3.1: *Chandra* ACIS-I effective area multiplied by a quantum efficiency correction and the response matrix (from the *Chandra* public archive web site).

Then, the flux is weighted by the ratio of the two, as follows:

$$S_{eff} = S_{meas} \times \left(\frac{CF_*}{CF}\right) \tag{3.4}$$

in which the effective flux S_{eff} is expressed in terms of the measured flux S_{meas} and inserted into the number counts evaluation.

3.3 Expected *Chandra* number counts

The results on number counts are presented in Figure 3.2, for both the $R(z)$ and the $R = const$ models. The counts refer to the 2-10 keV band at a detection flux-limit of $F_{lim} = 10^{-15} erg\ cm^{-2} s^{-1}$, i.e. the *Chandra* Deep Field South (CDFS) flux limit (see Section 3.4).
First of all, it must be noted that the effect of the instrumental response introduces a bias against AGN2 detection, so that the local ratio is highly reduced also in the $z < 1$ Universe and in the $R = const$ model.
The difference among the models emerges above $z > 2$, where the trend of the $R(z)$ model is opposite of the $R = const$ one, in the sense that, at high redshift, AGN1 outnumber AGN2, at odds with what should happen if local Universe sources ratios were valid whatever the redshift.
This leads to a strict prediction of the model about the lack of high redshift absorbed sources, that is expected to emerge from *Chandra* surveys, provided a statistically significant spectroscopically identified AGN sample is available. Unfortunately, this is not the case, so far. Yet, a few clues can be inferred from *Chandra* data supply, eventually giving hints for the viability of the trend proposed here, as discussed in the next section.

3.4 Comparison with observations

In order to face with the most recent and accurate X-ray data, *Chandra* observations are discussed.
In what follows, observations of *Chandra* Deep Field South (CDF, Tozzi et al. 2001), which is a deep pointing (300 ks) of a 0.1035 deg^2 region of the sky at a flux threshold of $F_{lim}(0.5 - 2keV) \sim 10^{-16} erg\ cm^{-2} s^{-1}$ and $F_{lim}(2 - 10keV) \sim 10^{-15} erg\ cm^{-2} s^{-1}$ is considered. 197 sources were detected, 124 of which in both bands, 22 only in the hard band and 51 only in

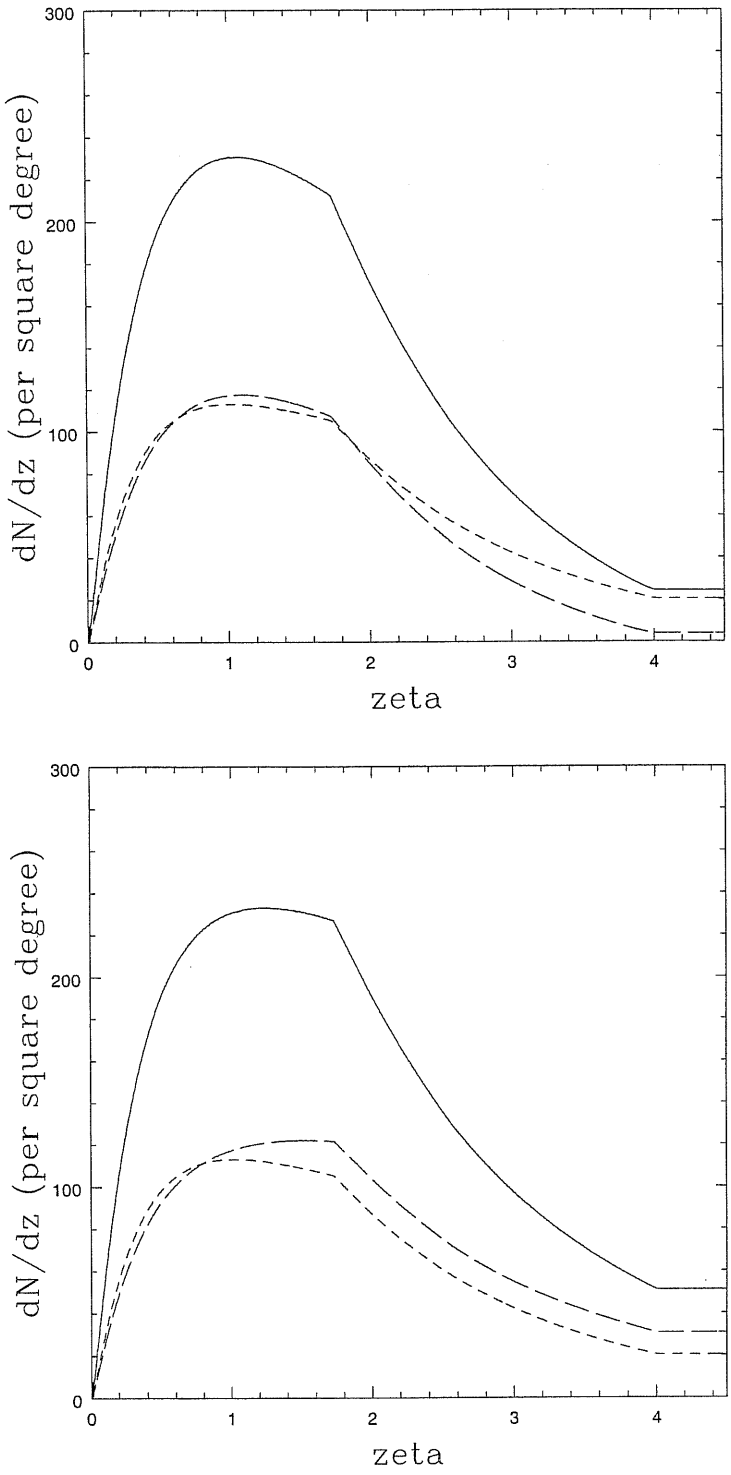

Figure 3.2: The number counts as a function of redshift in the present model (upper panel) and assuming $R = const$ (lower panel). Counts in the 2-10 keV band for AGN1 (short-dashed line) and AGN2 (long-dashed line) are reported, both with the total number (solid line) at a flux-limit of $F_{lim} = 10^{-15} erg\ cm^{-2} s^{-1}$.

the soft band; 86 redshifts were obtained.
The analysis of these data gives an important result that is worth being considered within the $R(z)$ model.
First of all, among the 86 sources for whom redshifts have been derived, the hardness ratio $HR \equiv \frac{H-S}{H+S}$ is found to be positive for sources located at $z \leq 1.6$, mainly $z < 1.0$. It implies that hard sources have lower redshift ($z \leq 1.0$). Besides, there is lack of a significant population of higher redshift absorbed sources, in contrast with other XRB synthesis models predictions, since they do expect a substantial contribution to the XRB by the so called type II QSO (Comastri et al. 1995; Gilli, Risaliti & Salvati 1999). This is confirmed by the 1 Million Second Exposure of the CDFS at a flux limit of $4.5 \times 10^{-16} erg\ cm^{-2} s^{-1}$ (Rosati et al. 2001), where AGN2 are found at a median redshift of $z = 0.8$, at odds with the mentioned XRB synthesis models. The authors ascribe this to different evolutionary scenarios for these sources, which could be troublesome for the UM. Actually, the introduction of $R(z)$ is exactly mimicking this effect, reducing the number of AGN2 at higher redshift.
The lack of absorbed sources in the high redshift Universe is underlined by Alexander et al. (2001) analysis of *Chandra* Deep Field North (CDFN) data, as well, where type II QSO are contributing to the XRB as a fraction much lower then the estimated $\sim 30\%$ (Gilli, Risaliti & Salvati 1999). It is important to note that their low detection can also be hardly reconciled with the prediction of hierarchical cold dark matter QSO formation models (Haiman & Loeb 1999).
Besides, this seems not to be due to flux limit / redshift combination bias. Indeed, the detection of sparse absorbed high redshift sources (e.g. a type II QSO, Norman et al. 2001) and the fact that their paucity extends up to very low flux limit ($4.5 \times 10^{-16} erg\ cm^{-2} s^{-1}$, Rosati et al. 2001) make the bias hypothesis weaker and the absence of high redshift absorbed sources could be real, as expected from the general trend of $R(z)$.
Though not definite, the above result is emerging in different *Chandra* observations (Barger et al. 2001; Brandt et al. 2001; Alexander et al. 2001) and the forthcoming spectroscopic identifications will be crucial to clarify this point.
An intriguing new result is coming from *Chandra* surveys, that is the presence of X-ray active galaxies and not yet identified X-ray sources, emerging at lower fluxes. As concerns the former, up to $\sim 10\%$ of optically luminous galaxies are retained to be X-ray active and their presence in *Chandra* fields

is indeed relevant (Barger et al. 2001).
A few important constraints about the latest issue were put forward by the Barger et al. (2001) *Chandra* Hawaii Deep Field Survey analysis. The sample is composed by 20 sources detected in the 2-10 keV. The authors obtained 13 identifications: 2 QSO, 5 AGNs, 6 early type galaxies. The 7 unidentified sources are consistent with intermediate redshift ($z = 1.5-3.0$) evolved early type galaxies.
It must be emphasized that just one third of detected sources have secure AGN identifications. Though not representative as a significant sample, nevertheless it agrees with other authors general result (Brandt et al. 2001) that a significant population other than AGN, including optically luminous galaxies, do appear at lower fluxes (see also Alexander et al. 2001).
An important caveat refers to the recently claimed observational evidence of two distinct population of AGN2. Despite the same optical classification, there seem to be a "standard" AGN2, i.e. hosting an obscured AGN1 nucleus, and "pure" AGN2, probably powered by a strong starbursts component.
On the other hand, the double AGN2 population hypothesis is supported by cross-correlation analysis of optical, infrared and X-ray catalogues (e.g. Tran 2001; Guainazzi et al. 2001), as well.
If this is the case, despite their optical classification, the non typical AGN2 do not *a priori* fulfill the UM model and the spectral characterization discussed in this work (Chapter 2). Therefore, they should be introduced as a new population, as well as the non AGN sources, in the XRB synthesis models, as discussed in the next section. The topic of the non AGN population and the possible existence of two types of AGN2 is also considered in Chapter 4.

3.5 XRB prediction

Turning to the XRB, other informations can be gained, since it can represent a more strict constraint with respect to the still incomplete information on number counts statistics.
The measured intensity of the 2-10 keV XRB by HEAO-1 data (Marshall et al. 1980; Gendreau et al. 1995) is $I_{XRB} = 1.6 \times 10^{-11} erg\ cm^{-2} s^{-1} deg^{-2}$ and *Chandra* has resolved a fraction between 60-90% of it between 10^{-13} $erg\ cm^{-2}\ s^{-1}$ and $10^{-15} erg\ cm^{-2} s^{-1}$ (Tozzi et al. 2001), the exact fraction depending on the possible underestimate of the 1 keV normalization, as reported by Vecchi et al. (1999) (the upper limit to it being $\sim$ 30 % higher,

according to MECS BeppoSAX measurements).
The present model produces for the AGN integrated emission $I_{XRB}^{AGN} = 9.5 \times 10^{-12} erg\ cm^{-2} s^{-1} deg^{-2}$, that is 60% of the measured HEAO-1 XRB intensity and nearly 80% of the resolved *Chandra* intensity. Therefore, 20% of the 2-10 KeV XRB observed by *Chandra* should be released by sources other than AGN.
On the other hand, at a flux-limit of $10^{-15} erg\ cm^{-2} s^{-1}$, the AGN number counts of the model provide nearly 600 deg^{-2} sources, corresponding to $\sim 1/3$ of the observed value in Tozzi et al. (2001), the fraction being slightly lower if Mushotzki et al. (2000) log N-log S normalization is considered. It means that no AGN X-ray sources are outnumbering AGN, which indeed seems to be the case, as reported by Barger et al. (2001), whose sample has $\sim 1/3$ secure AGN identifications.
Besides, if the relative space densities are considered, the picture emerging from the present model is that 40% of *Chandra* detected sources are AGN, emitting in the whole range $L_{AGN} = 10^{42} - 10^{45} erg\ s^{-1}$, while an outnumbering faint population spans the $10^{38} - 10^{41} erg\ s^{-1}$ range of luminosities, i.e. from X-ray binaries to giant ellipticals (see Table 3.1).
As concerns the AGN produced hard XRB, the main contribution is found to arise from $z < 1.5$ absorbed sources, i.e. low-redshift AGN2, still over abundant in that redshift range, which is consistent with AGN / X-ray sources redshift distribution tentatively inferred from observations (Alexander et al. 2001).
It must be noted that the 2-10 keV AGN logN-logS slope is found to be $\alpha = 0.73$, flatter than the whole population (AGN + other sources) slope reported by Tozzi et al. (2001), where $\alpha = 0.92$. It is likely that the steepening is provided by the faint no AGN population emerging at lower fluxes, though our model cannot make any quantitative prediction on it. On the other hand, it is important to recall that the CDFS slope is better described by a double power law shape, with a significant flattening at the faint end; besides, the slope in the 5-10 keV is much steeper (Rosati et al. 2001). This means that different X-ray populations are emerging in number counts in different bands and a clear separation of their contribution would be needed to compare the model prediction with the CDFS results, which is not at disposal so far.

As a last information which can be inferred by the present model, some clues on the accretion history can be found, as follows.
The AGN produced XRB is $I_{XRB}^{AGN} = 9.5 \times 10^{-12} erg\ cm^{-2} s^{-1} deg^{-2}$, which

Population	I_{XRB}	density	$L_X(erg\ s^{-1})$	redshift
AGN	< 0.60	< 0.40	$10^{42} - 10^{45}$	< 1.5
no AGN	> 0.40	> 0.60	$10^{38} - 10^{41}$	$1.0 - 3.0$

Table 3.2: The contribution of different X-ray populations (first column) to the 2-10 keV XRB (second column) and number density percentage (third column), with the relative luminosities (fourth column) and redshift ranges (fifth column).

corresponds to a bolometric value, if a conversion factor k is allowed, that is:

$$I_{AGN}(2 - 10\ keV) = k \times I_{AGN}(BOL). \tag{3.5}$$

The value of k is retained to be a few percent; in what follows, since the purpose here is to obtain an upper limit for the accretion efficiency, the lowest value for k as estimated by Barger et al. (2001) is used, namely $k = 0.03$.
With the above numbers, the bolometric energy density of the AGN producing the XRB radiation is found to be:

$$U = \frac{4\pi}{c} I_{AGN}(BOL) \simeq 9 \times 10^3 (M_\odot c^2)\ Mpc^{-3} \tag{3.6}$$

where the energy density has been written in terms of solar mass energy ($M_\odot c^2$) for later convenience.
Introducing the universal mass density of massive black holes ρ_{BH} and the mean redshift z of the sources producing the XRB, it holds:

$$\rho_{BH} = \frac{1+z}{\epsilon} \frac{U}{c^2} \tag{3.7}$$

where ϵ is the accretion efficiency, which is the task of the calculation.
Once the above value is evaluated, it can be compared to the estimate of the black hole mass density in the local Universe. According to Merrit & Ferrarese (2001):

$$\rho_{BH} = 5 \times 10^5 M_\odot Mpc^{-3}. \tag{3.8}$$

As a reference value for the AGN redshift, according to the $R(z)$ trend, a value in the range $z = 1.0 - 1.5$ can be used. Then, by comparing eq. (3.7) and (3.8), an upper limit of:

$$\epsilon \leq 5 \times 10^{-2} \tag{3.9}$$

can be set. It is important to note that if all the *Chandra* resolved 2-10 keV XRB where produced by AGN, the above value would shift to nearly ten per cent, in agreement with other models estimates (e.g. Gilli, Risaliti & Salvati 1999 model), whose upper limit is fifteen per cent, owing to the SED used to evaluate the value of k in eq. (3.5) (Risaliti, private communication). Nevertheless, the estimated accretion is quite efficient, so that low luminosity regimes, such as ADAF models, cannot be significantly active.
Then, the typical QSO ($L_{BOL} \sim 10^{45} erg\ s^{-1}$) accretion rate $\dot{M}_{BH}$ can be inferred as follows:

$$\dot{M}_{BH} = \epsilon^{-1} \frac{L_{BOL}}{c^2} \simeq 3.5 \times 10^{-1} M_{\odot} yr^{-1} \tag{3.10}$$

namely, a $\sim 10^8 M_{\odot}$ black hole can be formed through accretion in AGN over a $\sim$ Gyr time scale.
This result completes the set of informations the model can supply:

- **the XRB is mainly (up to 60 %) produced by low redshift ($z < 1.5$) and quite efficiently accreting AGN ($\epsilon \simeq 5 \times 10^{-2}$), most of them being AGN2;**
- **a three times higher population of X-ray sources spanning a wider range of redshifts is emitting with a much lower luminosity ($L < 10^{41} erg\ s^{-1}$) and provides the rest (~ 40 %) of the XRB.**

Chapter 4

Discussion and conclusion

4.1 The $R(z)$ model implications

The cornerstone of the model presented in this work is the redshift dependent AGN2 percentage ($R(z)$).
Actually, $R(z)$ adds to AGN2 a density evolution with respect to the PLE scenario for AGN1. This should be reconciled with the UM, which in principle predicts the same evolution for AGN1 and AGN2. On the other hand, UM as a viable first order scheme must be retained, as the observations of individual sources in the local Universe support.
It implies that an extra parameter not directly linked to orientation is relevant in AGN1/AGN2 classification and must be added to the UM picture.
The possibilities restrict to different environmental settings in AGN1 and AGN2, both in the host galaxy and in the surrounding.
Actually, statistical analysis of AGN1 + AGN2 samples do show results that are challenging for the UM. They mainly concern the host galaxy morphology and environment and are reviewed in Section 4.2.
In Section 4.3 an eventual theoretical framework to analyze the actual meaning of $R(z)$ is presented.
Before going deeper into the topic, it is important to remind that the general accepted model for AGN emission mechanism and physical structure relies on UM and that the purpose of this chapter is not to deny or disprove it, but to look for its possible extension. This is pursued in order to give an interpretation to the $R(z)$ factor and to give further support to observational data claiming for AGN1/AGN2 intrinsic differences.

4.2 Observational clues

Many recent studies have been devoted to disentangle statistically significant differences among type 1 / type 2 AGNs and further complications to the UM.
Two important issues that cannot be accounted for by the UM are:

1. host galaxies and environmental differences among AGN1 and AGN2 in Seyfert galaxies;

2. the existence of two different types of AGN2, i.e. a hidden AGN1 (as expected from the UM) and a "pure" AGN2.

It is worth recalling the main results on this two topics before relating them to the $R(z)$ model.
As concerns points 1., environmental effects seem to be relevant, in the sense that the relative densities of Seyfert 2 are up to a factor of three times higher than those of Seyfert 1 (Laurikainen & Salo 1995; Dultzin-Hacyan et al. 1999).
However, the most challenging results regard the host galaxies, which show differences in many physical characteristics, including:

- the Hubble type: Seyfert 1's is earlier than Seyfert 2's (Malkan et al. 1998; Hunt & Malkan 1999);

- the circumnuclear star-forming activity: there is more starburst activity in Seyfert 2 than in Seyfert 1 (Maiolino et al. 1997; Ohsuga & Umemura 1999);

- the bar percentage in Seyfert 2 is also higher than that Seyfert 1 (Pogge 1989; Maiolino et al. 1997).

It must be emphasized that the two effects, i.e. environment and host galaxies, could be linked, if a *reactivation scenario* for AGN phenomenon is considered (see Section 4.3). Indeed, if accretion within an AGN is induced by gravitational disturbance activating gas inflow, than, for instance, the presence of close companions or the incidence of minor/major encounters could affect the internal structure of the galaxy and therefore the accretion history (e.g. Storchi-Bergmann et al. 2001).
Turning to the possible existence of two Seyfert 2 types, it is a long-standing

conjecture (e.g. Antonucci 1993), originally motivated by IR (Hutchings & Neff 1991; Neff & Hutchings 1992) Radio (Moran et al. 1992) and UV observations (Heckman et al. 1995) and more recently extended to the X-rays. As concerns the X-rays, the issue has received new insight by studies on IR vs. hard X correlations (Tran 2001) and X-ray absorption vs. optical reddening (Guainazzi et al. 2001).
The main point about it is that there seems to be a "pure" Seyfert 2 type, which has no hidden Seyfert 1 nucleus. In other words, its luminosity is not produced by accretion onto a Supermassive Black Hole, but it is probably related to circumnuclear starbursts. In the "pure" Seyfert 2 sources, the mechanism obscuring the nucleus can be different, as well, since it should not be close to the core of the AGN (eventually associated with the molecular torus), but should arise on much larger scales (e.g. galactic dust lanes).
It is important to note that better inspection of the above Seyfert 2 conjecture is particularly relevant to have new hints about the starbursts/AGN connection. This is crucial for the proposed evolutionary sequence, according to which a starburst event turns a galaxy to a Seyfert 2 (Storchi-Bergmann et al. 2001; Mouri & Taniguchi 2001).
For the sake of completeness, it must be said that the results discussed in this section are not definite and should benefit of multi wavelength observations. Therefore, better constraints on the effectiveness of the statistical correlations can be tested as more data supply are available.
As a conclusion, from an observational point of view, the UM seems not to be the final solution. As a consequence, the present $R(z)$ model can support the necessity of an extension of the UM itself, a possible theoretical reasoning of which is sketched in the next Section.

4.3 A possible theoretical approach

A few theoretical hints can be given to analyze the above possibility.
If a short-lived scenario for the AGN phenomenon is considered, in which the AGN is a transient phase in a galaxy lifetime lasting $\tau_{AGN} \sim 10^8$ yr and eventually undergoing several reactivation events, then the kinetic equation approach (Cavaliere & Vittorini 2000 and references therein) is a well suited framework to infer the meaning of $R(z)$.
This approach describes the number of active sources through a continuity

equation:

$$\partial_t N + \partial_L \left(\dot{L} N\right) = S_+ - S_- \tag{4.1}$$

where ∂_t, ∂_L denote the partial derivatives with respect to the cosmic time t and the luminosity L.
The astrophysical and cosmological inputs, in which the nature of $R(z)$ eventually resides, are:

1. **the brightening term** $\rightarrow \dot{L} = \frac{L}{\tau}$;
2. **the source function** $\rightarrow S_+(L,t)$: it is the rate of reactivations per unit L and is proportional to the ratio of the surrounding number of galaxies to the reactivation time-scale $\frac{N_G(t)}{\tau_r(t)}$;
3. **the sink function** $\rightarrow S_-(L,t)$ representing the sources per unit time fading due to fuel consumption.

1. and 3. show time-scales inconsistency to be the leading cause, since they should be tuned in a systematic way in order to provide the general $R(z)$ trend to the overall population spanning over a wide range of redshift.
Therefore, the source function should be the main responsible for different AGN1/AGN2 evolution.
A general solution of the kinetic equation has the following shape (Cavaliere & Vittorini 2000):

$$N(L,t) = \tau_{AGN} \frac{N_G(t)}{\tau_r(t)} N(L) \tag{4.2}$$

where N_G denotes the number of over densities where AGN preferentially resides (e.g. groups of galaxies) and τ_r is the reactivation time scale of the AGN phenomenon.
If we suppose that $N_{AGN2}(L) = R \times N_{AGN1}(L)$, which is the easiest assumption according to the UM, and that the AGN phenomenon follows the same physical processes in AGN1 and AGN2, then the redshift dependence in the $R(z)$ factor is likely to reside in the term $\frac{N_G(t)}{\tau_r(t)}$.
Although just a qualitative argument, this would mean that:

the redshift variation of AGN2 / AGN2 percentage is related to differences and temporal modification, i.e. evolution, of the ratio among the over densities of sources around AGNs and the reactivation time scale for the two types of sources.

Again, we emphasize that $\tau_r(t)$ is linked to the host galaxy structure, while

$N_G(t)$ depends on the environment, so that their combination could be supported by the Seyfert1 vs. Seyfert2 statistical analysis mentioned above.
To have further inspection, an equivalent approach restates eq. (4.1) as a conservation equation (Small & Blandford 1992):

$$\partial_t N(M,t) + \partial_M \left(N(M,t)\langle \dot{M} \rangle \right) = S(M,t) \tag{4.3}$$

where the first term describes the temporal evolution of the number density, the second one relates evolution to mass variation (through accretion) and the right hand side introduces a source function $S(M,t)$.
According to the reactivation scenario, an AGN undergoes several episodic duty-cycles of activity. If it is assumed that a duty-cycle lasts a fraction $\delta(M,t)$ of the galaxy lifetime and the accretion efficiency ϵ and Eddington parameter λ and time t_E are introduced, such that the luminosity is:

$$L = \lambda \frac{M}{t_E} c^2 = \epsilon \dot{M} c^2 \tag{4.4}$$

then, the average accretion rate is given by:

$$\langle \dot{M} \rangle = \frac{\lambda M \delta(M,t)}{\epsilon t_E} \tag{4.5}$$

with typical values of $\lambda \sim 0.1$ for a radio-quiet object (Sanders, Scoville & Soifer 1991), $\epsilon \sim 10^{-2}$ (see Section 3.5) and $t_E \simeq 4 \times 10^8$ yr.
Eq.(4.3) can be written introducing the XLF Φ, the duty-cycle δ and the new variable $\tau \equiv \frac{\lambda t}{\epsilon t_E}$ as:

$$\partial_\tau \left(\frac{\Phi}{\delta} \right) + L \partial_L \Phi = 0. \tag{4.6}$$

If an Einstein-de Sitter Universe is considered, the above relation becomes:

$$\partial_z \left(\frac{\Phi}{\delta} \right) = \frac{3\lambda t_H}{2\epsilon t_E} (1+z)^{-5/2} L \partial_L \Phi \tag{4.7}$$

for a Hubble time t_H.
Again, any differences among AGN1 and AGN2 should be imprinted in the solution of the above equation. Albeit observational limitations and uncertainties, from a purely theoretical point of view, the knowledge of AGN1 XLF should allow the determination of the reactivation history, namely the duty-cycle functional shape $\delta(M,t)$. Then, AGN2 parameters could be retrieved, following one of the approaches below:

- AGN2 XLF is the same that AGN1 XLF: any differences in $\delta(M,t)$ can be inferred;
- AGN2 $\delta(M,t)$ is the same that AGN1 XLF: any differences in AGN2 XLF can be inferred.

Actually, the first one is more directly related to environmental/triggering connection in AGN1/AGN2 reactivation events, as discussed in the previous Section. On the converse, the second hypothesis is more dramatic with respect to the UM.
As a last remark, eq.(4.3) can be directly related to $R(z)$ if the second approach proposed above is pursued and if $R(z)$ is introduced as a pure density evolution term, i.e. $\Phi_{AGN2} = R(z) \times \Phi_{AGN1}$. For instance, the AGN2 source function should fulfill:

$$\Phi(L,z)\partial_z R(z) + [1+R(z)]\left[\partial_z \Phi(L,z) + \partial_L\left(\Phi(L,z)\partial_z L\right)\right] = S(M,t) \quad (4.8)$$

where $\Phi(L,z)$ is the measured AGN1 XLF.
Nevertheless, it must be stressed that this Section is intended just to give an overview of a possible theoretical framework, which needs a strict treatment that is beyond the scope of this work.

4.4 A new X-ray population

One of the most unexpected and interesting result from X-ray surveys at low flux limit has been the discovery of a significant population of X-ray sources, other than AGN, emerging at fainter fluxes and spanning a remarkable range in luminosity and redshift.
It is needed to recall that *new X-ray population* in this concern means X-ray sources different from standard luminosity Seyfert galaxies or QSOs.
The issue of securely identifying this class of objects involves both observational (i.e. spectroscopy) and theoretical effort and it seems to be, at the moment, a priority challenge in X-ray astronomy.
So far, a few hints about the no AGN population can be put forward.
As a first reasonable guess, those new sources could be normal galaxies whose X-ray activity should be due to a low-luminosity AGN or to integrated emission of discrete galactic sources (e.g. X-ray binaries, Supernovae remnants). Specifically, nearly $\sim$ 7 % of optically bright galaxies show X-ray activity

(Barger et al. 2001) and belong to this new class, though their estimated surface density can only cover less than half the gap between AGN and total number counts.
On the other hand, a relevant amount of optically faint galaxies ($I \geq 24$) has been found in CDFN (Alexander et al. 2001), though their actual nature is under investigation. Indeed, their optical to near IR colors and X-ray to optical flux ratios generally allow them to be dust extincted and/or $z > 1$ normal galaxies, as well as $z < 3$ absorbed AGN. In a few objects, available variability data can help to disentangle that point, but in general both possibilities must be kept in mind.
So far, general consensus has been reached about the presence of a bimodal distribution of sources in the X-ray deep surveys:

1. an optically faint population with relatively blue colors;

2. an optically brighter class with much redder colors.

This is emerging in CDFS, as well, where the faint population seems to host $z \sim 1-2$ AGN2, while the brighter one is dominated by normal galaxies or low-luminosity AGNs (Koekemoer et al. 2001).
It must be noted that theoretical models on discrete integrated X-ray emission mainly produced by X-ray binaries in normal galaxies, as follows from a peak in star formation rate at $z > 1$, give a number of sources comparable to the required fraction to fill in the gap between AGN and total number counts. Besides, normal galaxies are predicted to dominate the total X-ray logN-logS at fluxes below $10^{-17} - 10^{-18} erg\ cm^{-2} s^{-1}$ (Ptak et al. 2001).
A last remark concerns the fact that the approach used in this work was relying on the UM to estimate AGN contribution to the XRB, so that it is lacking the possibility of a second AGN2 population. If this is the case, this population should have two main characteristics:

- it is not fulfilling the UM paradigm;

- the combination of spectral properties and redshift distribution is suitable to mimic the XRB shape.

The inclusion of this extra class of sources could explain part of the mentioned gap in number counts, although normal galaxies should play a major role in it.

4.5 Conclusions and perspectives

The XRB in the hard band is generally believed to be produced by AGN1 / AGN2 integrated emission. In agreement with this, a model involving observed AGNs spectra and fitting the XRB has been proposed.
It mainly shows up the necessity of a redshift dependent AGN2 percentage and such a result has been applied to predict number counts statistics. Both theoretical and observational predictions have been obtained.
We underline that the model could be tested only with wide surveys data (i.e. high statistics), while no definite conclusion can be reached just on the basis of deep fields (i.e. low flux-limit) number counts.
Nevertheless, a comparison with preliminary *Chandra* data on X-ray sources has been pursued and the X-ray sky description as follows from the model has been sketched.
When facing *Chandra* data, the most notable result we emphasize is that the X-ray sky is deeply populated by sources other than standard AGNs.
The true nature of this class of sources is still a challenging issue, which will hopefully gain more inspection by future data supply.
As a conclusion, the basic findings about the XRB / AGN connection that the proposed model can put forward are:

- **AGNs cannot account for the total XRB intensity in the hard band, neither they can reproduce the total hard band number counts;**
- **the UM is not the whole story, since further differences than orientation effects are present (introduced into the model by the $R(z)$ factor).**

Then, it seems that the long-standing paradigm for the synthesis of the hard XRB through AGN emission is no more a complete recipe, but it needs to be refined.
Further tests to the UM and inspections of the newly discovered X-ray sources play the key role in that goal. Two possible future extensions of this work are worth considering:

- the improvement of the hard XLF determination and an independent estimate of the AGN2 hard XLF;
- further constraints on the nature of AGN2 from IR data.

These two points are briefly discussed in what follows.

4.5.1 The hard XLF and AGN2 XLF

As mentioned in Chapter 2, the $R(z)$ model is deeply dependent on the choice of the XLF and the possible AGN1/AGN2 XLF mismatch.
The XLF is crucial for the functional shape of $R(z)$ and the steep decrease found in this work could change if a significant modification to the XLF is introduced. Therefore, a more accurate determination of the hard XLF is crucial and the availability of an AGN2 XLF would greatly help to test the UM.
A new inspection in this topic is coming from the analysis of BeppoSAX HELLAS survey data, performed by the author in collaboration with the HELLAS consortium (La Franca et al 2001, in preparation). Preliminary results can be found in La Franca et al. (2000) and La Franca et al. (2001). The HELLAS sample consists of 118 sources in the flux range of $3 \times 10^{-14} - 10^{-12} erg\ cm^{-2} s^{-1}$ in the 2-10 keV band and, to date, spectroscopic identifications have found 37 AGN1 and 9 AGN2 (the rest of the identified sources are 5 Narrow Line Emission Galaxies, 6 Clusters, 2 BL Lac, 1 Radio Galaxy and 1 star).
Unfortunately, this is not enough to gain a statistically significant AGN2 XLF, so that this issue must wait for further identifications and cannot be discussed, so far.
On the other hand, a new evaluation of the AGN1 XLF in the 2-10 keV has been performed, adding respectively 84, 12 and 25 AGN1 from the 2-10 keV samples of Grossan (1992), Boyle et al. (1998) and Akyiama et al. (2000) to the HELLAS sample.
From the total sample (157 AGN1 in the $0 < z < 3.0$ range), a few results were found:

- with respect to previous estimates, an excess of faint AGN1 at redshifts larger than $z \sim 0.3$ is found;
- the evolution is slightly slower than previously established in PLE models ($k = 2.12$) and stops earlier ($z_c = 1.39$);
- the slopes are not significantly different ($\gamma_1 = 1.87$, $\gamma_2 = 3.03$), but the break luminosity is higher ($log\ L^* = 44.17$).

A comparison among the Boyle et al. (1994) and the HELLAS XLF is reported in Fihure 4.1. The main difference regards the faint end normalization, which is higher in the HELLAS XLF. This should imply a steeper $R(z)$ trend. However, the bulk of the sources are located around the break luminosity, which corresponds to a lower density value in the HELLAS XLF, so that this effect counterbalances the previous one. In other words, the new XLF is not likely to make any dramatic difference in the results discussed in this work, even though a quantitative inspection of this is planned as a next task.
Another interesting result about HELLAS XLF is that a slightly better fit can be achieved if a LDDE model is considered. Besides, if a simple linear relation is assumed among the luminosities in the 0.5-2 keV and 2-10 keV bands, then the HELLAS (LDDE) XLF can be compared to the XLF (LDDE) derived by Miyaji, Hasinger & Schmidt (2000): this is done in Figure 4.2.It is clear from the figure that the strongest difference concerns the faint end and increases as redshift becomes larger.
Yet, the difference affects the part of the XLF where the data are not sufficient to constrain it and the observational results become poorer as higher redshifts are sampled. Therefore, this limitation does not allow to reasonably infer the consistency of the two LDDE models.
Unfortunately, the paucity of faint end sampling prevents from disentangling whether PLE or LDDE is a better description of the data.
Anyhow, a preliminary conclusion is that the $R(z)$ model should keep its basic trend, so that, as far as AGN evolution is concerned, breaking news could in case only come from the estimate of AGN2 XLF.
From the above discussion, it is clear that new insights in the XRB and the UM could mostly benefit from further information on AGN2, both from an evolutionary and a physical point of view. The latter means that new clues on physical structure of AGN2 (e.g. the actual existence of a "hidden AGN1" vs. a "pure" AGN2) are worth being retrieved.
An important tool in the last issue could come from IR data, which is discussed in the next Section.

4.5.2 IR observations of AGN2

Several studies on AGN2 have been based on IR data. This is due to the fact that the emission coming from the molecular torus arises in the IR. The nuclear continuum is absorbed by gas and dust located in the torus and the

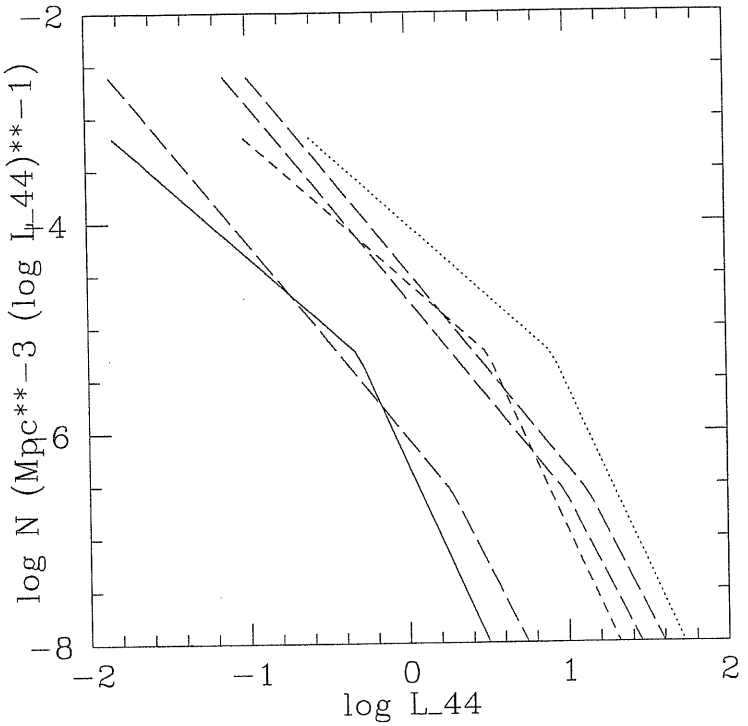

Figure 4.1: The XLF from the HELLAS sample (long-dashed lines) compared to the XLF from Boyle et al. (1994) at different redshifts: $z = 0.1$ (solid line); $z = 1.0$ (short-dashed line); $z = 3.0$ (dotted line).

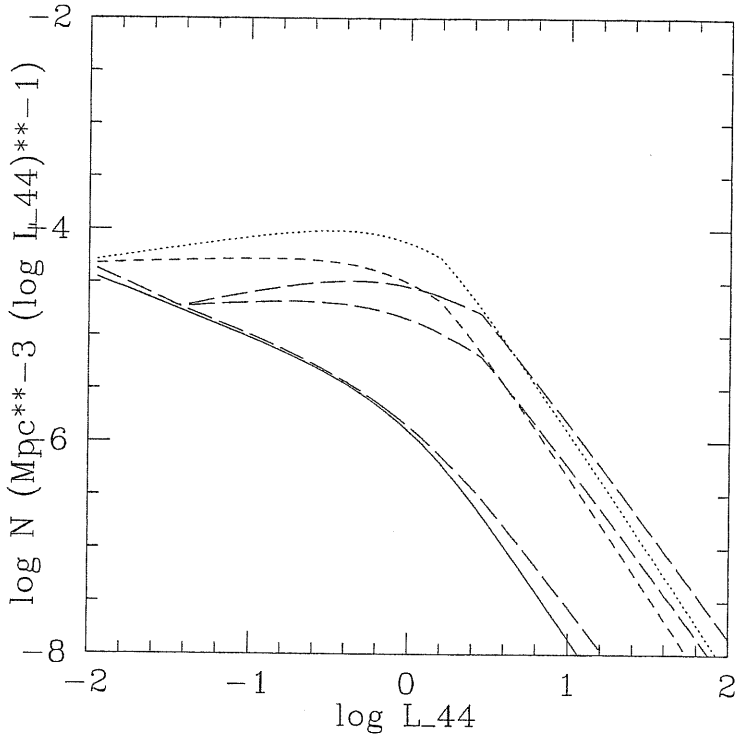

Figure 4.2: The XLF from the HELLAS sample (long-dashed lines) compared to the XLF from Miyaji, Hasinger & Schmidt (2000) at different redshifts: $z = 0.1$ (solid line); $z = 1.0$ (short-dashed line); $z = 3.0$ (dotted line).

dust is heated and emits as a black/grey body at characteristic temperatures. Many models have been proposed for the torus-like dust configuration (e.g. Efstathiou & Rowan-Robinson 1990; Pier & Krolik 1992; Granato & Danese 1994 among others). In these models the authors tried to constrain the physical parameters of the torus (e.g. dimensions and geometry, optical depth, dust distribution and properties) from the observed Spectral Energy Distribution (SED) of AGNs in the near IR bands (J, H, K, L, M), where the bulk of dust emission from the torus emerges.
A wealth of information has been found through such studies, mainly supporting the UM. For instance, the existence of the torus has been reasonably proved by fitting the observations with the mentioned models and its role in obscuring the nucleus has been inspected.
As far as this work is concerned, the main target with respect to IR would be to disentangle the existence of two types of AGN2, that is, if this is the case, to separate "hidden AGN1" AGN2 from "pure" AGN2. Anyhow, the goal would be to characterize as close as possible different physical processes and structures eventually being present in AGN2, by means of IR data.
This aim is undergoing in other wavelengths, as mentioned before. For instance, from optical data, a study of the incidence of hidden broad line regions (Tran 2001) or the search for host galaxy peculiar structures (e.g. dust lanes) from HST morphology (Guainazzi et al. 2001) have attempted to focus on the presence of the hidden nucleus and the place and structure of the obscuring medium. On the other hand, in the literature, other hints to this task come from the study of possible bimodality in the radio power distribution of AGN2 (Moran et al. 1992) or in the far IR color-luminosity plot (Neff & Hutchings 1992).
Further analysis in the IR could be based on many different approaches. Here, the use of diagnostic plots about near IR / HX and [OIII] flux and/or luminosity correlations is briefly discussed.
HX and [OIII] probe the nuclear continuum, while near IR is representative of torus dust emission, with the "warmer" colors being produced by the inner surface of the torus and the color becoming "cooler" as the external boundary is approached.
Correlations in these plots have long been known and studied (e.g. Mulchaey et al. 1994) for both AGN1 and AGN2 and discussed separately for the two types of sources.
These diagnostics could be a good tool to see whether any classified AGN2 deviates from the expected trend, which would mean that IR emission is not

emerging mainly from a inner torus-like configuration: this would prevent the source from being dominated by a "hidden AGN1".
A few preliminary inspections, which are part of a work going on in collaboration with G. Granato, are described below.
The AGN2 sample of Alonso-Herrero et al. (2001) is considered. The sample is composed by 12 AGN2, for which J, H, K, L', M and ISO (12, 25, 60 and 100 μm) data are available. In addition, data for hard X-rays (2-10 keV) and [OIII] fluxes can be found in Bassani et al. (1999) with the corresponding estimate for the neutral hydrogen column density (N_H).
The reason to consider this sample of AGN2 is twofold.
First, the sample is composed by Compton-thin AGN2, apart from NGC1068 ($N_H > 10^{25} cm^{-2}$). This is particularly appealing, since the most intriguing sources with particular structures which could violate the UM are mainly found among Compton-thin sources (Guainazzi et al. 2001). Second, the Alonso-Herrero et al. (2001) sample provides good quality data in all the NIR bands and, noticeably, an estimate of the flux nuclear component, i.e. coming from the AGN, and non-nuclear component, i.e. coming from the host galaxy, is given.
In Figure 4.3-4.6 some basic diagnostic plots are reported. The analysis of them rests on the assumption that the [OIII] and the hard X-ray fluxes are isotropic properties and therefore represent the intrinsic power of AGN, and the simple assumption that the opening angle of the ionization cone is similar in both AGN1 and AGN2. Support for the former hypothesis comes from the similarity of the hard X-ray and [OIII] luminosities in both types of AGN (Mulchaey et al. 1994).
The choice of the L' band in the diagnostics is due to the fact that it is not deeply affected by stellar emission. Indeed, the correlations become poorer as the bands from K to J are considered, where stars can be dominant.
Though limited by the paucity of sources, a tentative trend can be seen in the plots. In particular, most of the sources seem to cluster around a linear correlation. This is more evident in the flux vs. flux plots, due to the uncertainties introduced by the estimate of the AGN distance in the luminosity plots. The fact that the trend is present both in HX and [OIII] plots is not unexpected, since HX and [OIII] are known to be correlated and indeed they are used to calibrate a well-studied relation providing an estimate of the intrinsic nuclear power (Bassani et al. 1999).
Actually, a linear correlation in both HX$\times L$, [OIII]$\times L$ for AGN1 was found by Alonso-Herrero, Ward & Kotilainen (1997). According to these authors,

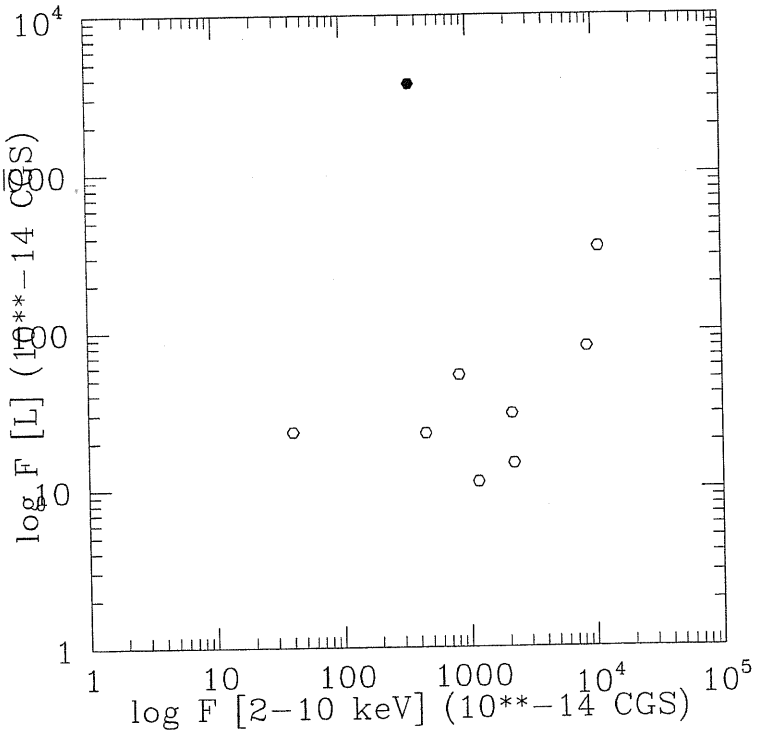

Figure 4.3: The hard X (2-10 keV) versus the L' band fluxes (units of $10^{-14} erg\ cm^{-2} s^{-1}$) for the AGN2 sample of Alonso-Herrero et al. (2001). The filled dot refers to NGC1068.

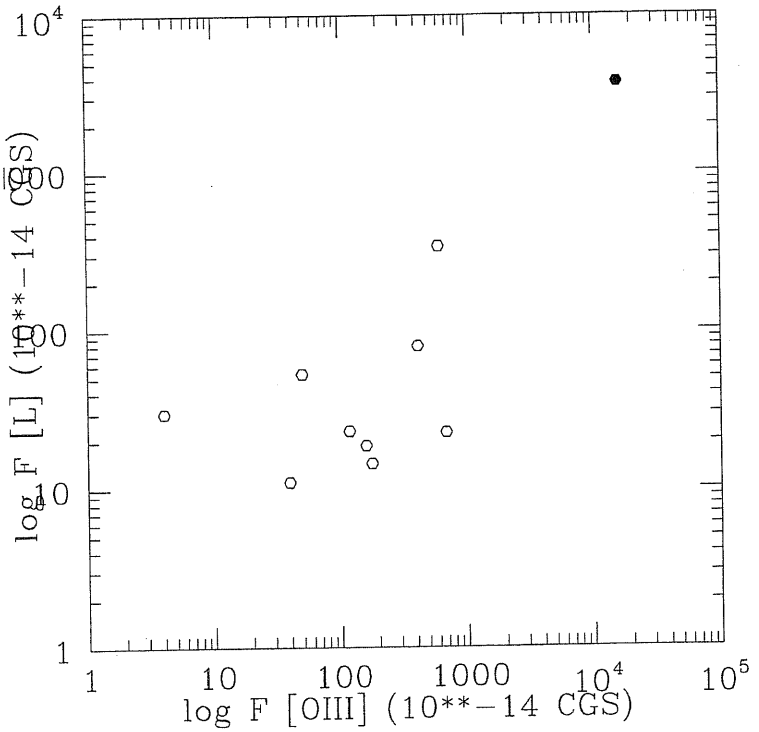

Figure 4.4: The [OIII] versus the L' band fluxes (units of $10^{-14} erg\ cm^{-2} s^{-1}$) for the AGN2 sample of Alonso-Herrero et al. (2001). The filled dot refers to NGC1068.

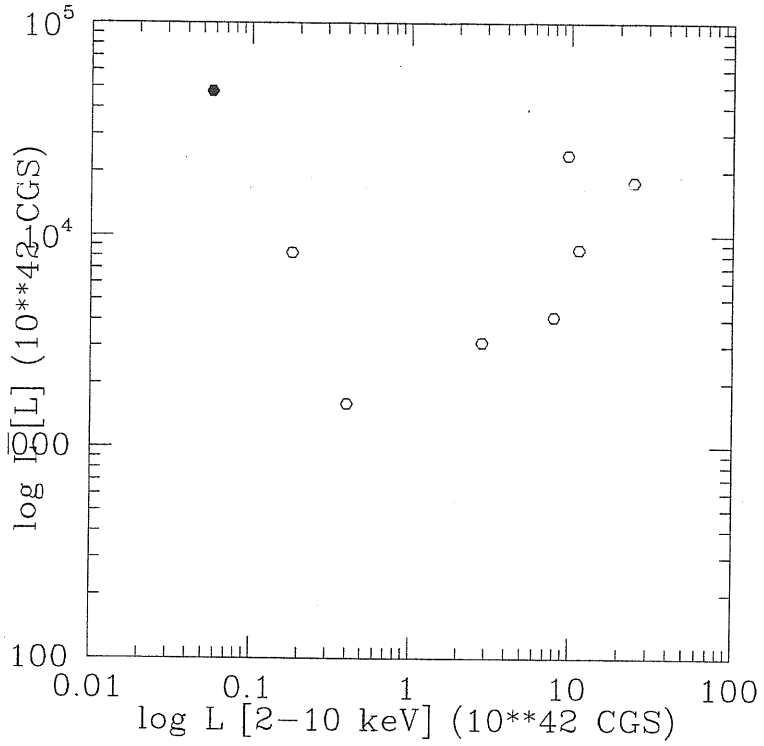

Figure 4.5: The hard X (2-10 keV) versus the L' band luminosities (units of $10^{42} erg\ s^{-1}$) for the AGN2 sample of Alonso-Herrero et al. (2001). The filled dot refers to NGC1068.

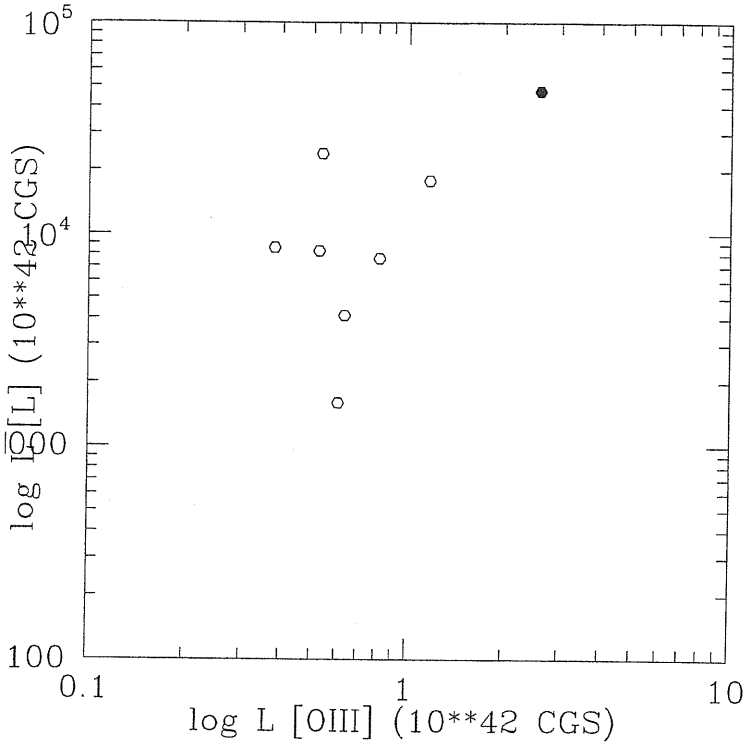

Figure 4.6: The [OIII] versus the L' band luminosities (units of $10^{42} erg\ s^{-1}$) for the AGN2 sample of Alonso-Herrero et al. (2001). The filled dot refers to NGC1068.

the position in the plot departs from the linearity region as the N_H increases and the AGN1 turns to an AGN2, the lack of correlation being higher for Compton-thick sources. This should be ascribed to the fact that the L band emission from the torus arises from the inner part of it, i.e. the "warmer" dust. Therefore, the L flux is angle-dependent: the more inclined the system, the less the L flux. In other words, the more inclined systems, namely the Compton-thick sources, will have most of the L band emission not coming from the torus, but from the circumnuclear region.
As concerns the Alonso-Herrero et al. (2001) sample, it is found that a few sources populate a region of the plot which is unexpected owing to their low value of N_H. In Figure 4.3-4.6 is also reported the Compton-thick source NGC1068 (black dot), in order to clarify how the correlation breaks up as the value of N_H becomes high enough.
It must be stressed that the possible stellar contamination from the host galaxy in the NIR bands could affect the plots. Nonetheless, it is minimized by Alonso-Herrero et al. (2001) by means of the small aperture observations and through the separation of AGN / host galaxy contributions.
At the moment, the analysis the plots are undergoing follows this procedure:

- look for "strange" sources, i.e. AGN2 deviating from the expected trend in the NIR / L band vs. hard X / [OIII] plots;
- try to fit their NIR emission with a torus model (Granato & Danese 1994) to see whether they are consistent with a standard "hidden AGN1" scenario or if any additional source of IR radiation is relevant.

Yet, the strongest limitation of such an analysis is the poor statistics and a more extended sample is needed to infer quantitative results.
As a concluding remark, it is worth stressing that the conjecture of the existence of two types of AGN2 is highly debated, at the moment. The fact that AGN2 are more elusive to detect than AGN1 limits their study and this is basically the reason way any claim about AGN2 needs to be carefully considered and some recent results have been questioned (e.g. Antonucci 2001).

Bibliography

[1] Akyiama M., Ohta K., Yamada T. et al. 2000, ApJ, 532, 700

[2] Alexander D.M., Brandt W.N., Hornscheimer A.E. et al. 2001, ApJ in press, astro-ph/0107450

[3] Allen K., Plucinski P.P., McNamara B.R. et al. 1998, in "Analysis of the AXAF HRMA+ACIS Effective Area Measurements from the XRCF", SPIE, Vol.3444

[4] Alonso-Herrero A., Ward M.J. and Kotilainen J.K. 1997, MNRAS, 288, 977

[5] Alonso-Herrero A., Quillen A.C., Efstathiou A. and Ward M.J. 2001, AJ, 121, 1369

[6] Antonucci R.R.J and Miller J.S. 1985, ApJ 297, 621

[7] Antonucci R.R.J 1993, ARA&A, 31, 473

[8] Antonucci R.R.J 2001, in the Proceedings of the IAU Colloquium 184, AGN Surveys, June, 18-22 2001, Byurakan, Armenia, astro-ph/0110343

[9] Barger A.J., Cowie L.L., Mushotzky R.F. and Richards E. A 2001, ApJ, 121, 662

[10] Bassani L., Dadina M., Maiolino R. et al. 1999, ApJS, 121, 473

[11] Boldt E. 1987, in the Proceedings of the IAU Symposium, held in Bejing, China

[12] Boyle J., Shanks T., Georgantopoulos I.G., Stewart G.C. and Griffiths R.E. 1994, MNRAS 271, 639

[13] Boyle B.J., Georgantopoulos I.G., Blair A.J. et al. 1998, MNRAS, 296, 1

[14] Brandt W.N., Hornschemeier A.E., Alexander D.M. et al. 2001, AJ in press, astro-ph/0102411

[15] Cavaliere A. and Vittorini V. 2000, ApJ, 543, 599

[16] Celotti A., Fabian A.C., Ghisellini G. and Madau P. 1995, MNRAS 277, 1169

[17] Chen L.-W., Fabian A.C. and Gendreau K.C. 1997, MNRAS, 285, 449

[18] Comastri A., Setti G., Zamorani G. and Hasinger G. 1995, A&A 296, 1

[19] Della Ceca R., Castelli G., Braito V. et al. 1999, ApJ, 524, 674

[20] Efstathiou A. and Rowan-Robinson M. 1990, MNRAS, 245, 275

[21] Fabian A.C. & Barcons X. 1992, ARA&A, 30, 429

[22] Fabian A.C. 1999, MNRAS, 308, L39

[23] Gendreau K.C., Mushotzky R.F., Fabian A.C. et al. 1995, PASJ, 47, L5

[24] Giacconi R., Gursky H., Paolini F. and Rossi B. 1962, *Phys.Rev.Lett.*, 9, 439

[25] Giacconi R., Rosati P., Tozzi P. et al. 2001, ApJ submitted, astro-ph/0007240

[26] Gilli R., Comastri A., Brunetti G and Setti G. 1999, *New. Astron.*, 4, 45

[27] Gilli R., Risaliti G. and Salvati M. 1999, A&A, 347, 424

[28] Gilli R., Salvati M and Hasinger G. 2001, A&A, 366, 407

[29] Giommi P., Perri M. and Fiore F. 2000, A&AS, 362, 799

[30] Granato G. and Danese L. 1994, MNRAS, 268, 235

[31] Grossan B.A. 1992, PhD Thesis, MIT

[32] Guainazzi M., Fiore F., Matt G. and Perola G.C. 2001, MNRAS in press, astro-ph/0106150

[33] Dultzin-Hacyan D., Krongold Y., Fuentes-Guridi I. and Marziani P. 1999, ApJL, 513, 111

[34] Haiman Z. and Loeb A. 1999, ApJ, 521, L9

[35] Hasinger G. 1992, in "The X-Ray Background", Barcons X. & Fabian A.C. Eds.

[36] Hasinger G., Altieri B., Arnaud M. et al. 2001, A&A, 365, L45

[37] Heckman T.M., Krolik J., Meurer G. et al. 1995, ApJ, 452, 549

[38] Hunt L.K. and Malkan M.A. 1999, ApJ, 516, 600

[39] Hutchings J.B. and Neff S.G. 1991, AJ, 101, 434

[40] Koekemoer A.M., Grogin N.A., Schreier E.J. et al. 2001, to appear in ApJ, astro-ph/0110385

[41] Kondo 1990, PhD Thesis, University of Tokyo

[42] Koyama K. 1989, PASJ, 41, 665

[43] La Franca F., Fiore F., Vignali C. et al. 2000, astro-ph/0011008, to appear in the Proc. of the Conference "The New Era of Wide-Field Astronomy", held in Preston (UK), 21-24 August 2000

[44] La Franca F., Matute I., Fiore F. et al. 2001, astro-ph/0109308, to appear in the Proc. of the Conference "Issues in Unifications of AGN", Maiolino R., Marconi A. & Nagar N. Eds.

[45] Laurikainen E. and Salo H. 1995, A&A, 293, 683

[46] Madau P., Ghisellini G. and Fabian A.C. 1994, MNRAS 270, L17

[47] Maiolino R. and Rieke G.H. 1995, ApJ, 454, 95

[48] Maiolino R., Ruiz M., Rieke G.H. and Papadopoulos P. 1997, ApJ, 485, 552

[49] Malkan M.A., Gorjian V. and Tam R. 1998, ApJS, 117, 25

[50] Marshall F.L., Boldt E.A., Holdt S.S. et al. 1980, ApJ, 235, 4

[51] Mather J.C., Cheng E.S., Eplee R.E. et al. 1994, ApJ, 420, 439

[52] Matt G. and Fabian A.C. 1994, MNRAS, 267, 187

[53] Matt G. 1998, in The Active X-Ray Sky, Scarsi L., Bradt H., Giommi P. and Fiore F. Eds., North Holland

[54] Matt G., Pompilio F. and La Franca F. 1999, *New. Astron.*, 4, 191

[55] Merritt D. and Ferrarese L 2001, MNRAS, 320, 30

[56] Miyaji T., Hasinger G. and Schmidt M. 1998, in Highlights in X-ray Astronomy in Honor of Joachim Treumper's 65th birthday, MPE Report, MPE, Garching

[57] Miyaji T., Hasinger G. and Schmidt M. 2000, A&A, 353, 25

[58] Moran E.C., Halpern J.P., Bothun G.D. and Becker R.H. 1992, AJ, 104, 990

[59] Mouri H. and Taniguchi Y. 2001, ApJ in press, astro-ph/0106155

[60] Mulchaey J.S., Koratkar A., Ward M.J. et al. 1994, ApJ, 436, 586

[61] Mushotzky R.F., Cowie L. L., Barger A.J. and Arnaud K. A. 2000, Nature, 404, 459

[62] Nandra K. and Pounds K.A. 1994, MNRAS, 268, 405

[63] Nandra K., George I.M., Mushotzky R.F. et al. 1997, ApJ, 476, 70

[64] Neff S.G. and Hutchings J.B. 1992, AJ, 103, 1746

[65] Norman C., Hasinger G., Giacconi R. et al. 2001, astro-ph/0103198

[66] Ogasaka Y., Kii T., Ueda Y. et al. 1998, *Astron.Nachr.*, 319, 430

[67] Ohsuga K. and Umemura M. 1999, ApJ, 521, L13

[68] Peebles P.J.E. 1993, Principles of Physical Cosmology, Princeton Univ. Press

[69] Perri M. and Giommi P. 2000, A&A, 362, L57

[70] Pier E. and Krolik J. 1992, ApJ, 401, 99

[71] Pogge R.W. 1989, ApJ, 345, 730

[72] Pompilio F., La Franca F. and Matt G. 2000, A&A, 353, 440 (PLM00)

[73] Ptak A., Griffiths R., White N. and Ghosh P. 2001, ApJ, 559, 91

[74] Risaliti G., Maiolino R. and Salvati M. 1999, ApJ, 522, 157

[75] Rosati P., Tozzi P., Giacconi R., Gilli R. et al. 2001, ApJ in press, astro-ph/0110452

[76] Rothschild R.E., Baity W.A., Gruber D.E. et al. 1983, ApJ, 269, 423

[77] Sanders D.B., Scoville N.E. and Soifer B.T. 1991, ApJ, 370, 158

[78] Schwartz 1992, in "The X-Ray Background", Barcons X and Fabian A.C. Eds., Cambridge Univ. Press

[79] Setti G. and Woltjer L. 1989, A&A, 224, 21

[80] Small T.A. and Blandford R.D. 1992, MNRAS, 259, 725

[81] Storchi-Bergmann T., Gonzalez-Delgado R.M., Schmitt H et al. 2001, astro-ph/0105538

[82] Tanaka Y. and Bleeker J.A.M. 1977, *Space Sci. Rev.*, 20, 815

[83] Takahashi Y., Ueda Y., Ishisaki Y. et al. 1998, *Astron.Nachr.*, 319, 91

[84] Tozzi P., Rosati P., Nonino M. et al. 2001, astro-ph/0103014

[85] Turner T.J. and Pounds K.A. 1989, MNRAS, 240, 833

[86] Tran H.D. 2001, ApJ, 554, 19

[87] Ueda Y., Takahashi T., Inoue H et al. 1998, *Nature*, 391, 866

[88] Ueda Y., Takahashi T., Inoue H et al. 1999a, ApJ, 518, 656

[89] Ueda Y., Takahashi T., Ishisaki Y. et al. 1999b, ApJ, 524, L11

[90] Vecchi A., Molendi S., Guainazzi M. et al. 1999, A&A, 349, 73

[91] Wang Q.D. and McCray R. 1993, ApJ, 409, L37